Sterility-Independent Enhancement of Proteasome Function via Floxuridine-Triggered Detoxification in *C. elegans*

Abhishek Anil Dubey[1], Natalia A. Szulc[1], Małgorzata Piechota[1], Remigiusz A. Serwa[2], Wojciech Pokrzywa[1,*]

1 Laboratory of Protein Metabolism, International Institute of Molecular and Cell Biology in Warsaw, 4 Ks. Trojdena Str., 02-109 Warsaw, Poland

2 International Institute of Molecular Mechanisms and Machines (IMol), Polish Academy of Sciences, M. Flisa 6, 02-247 Warsaw, Poland

* For correspondence: wpokrzywa@iimcb.gov.pl

ABSTRACT

The ubiquitin-proteasome system (UPS) functionality is vital for proteostasis, contributing to stress resilience, lifespan, and thermal adaptability. In *Caenorhabditis elegans*, proteasome constituents such as the RPN-6 and PBS-6 subunits or the PSME-3 activator are respectively linked to heat resistance, longevity at moderate cold (15°C), and survival at low temperatures (4°C). Since the inhibition of germline stem cells proliferation is associated with robust proteostasis in worms, we utilized floxuridine (FUdR), a compound known for inducing sterility, to examine whether it could reinforce UPS under proteasome dysfunction, particularly to foster cold survival. We demonstrate that FUdR promotes proteasome resilience during its inhibition or subunit deficits, supporting normal lifespan and facilitating adaptation to cold. FUdR's elevation of the UPS activity occurs independently of main proteostasis regulators and is partly driven by SKN-1-regulated transcription, especially under reduced proteasome function. Additionally, we uncover a FUdR-stimulated detoxification pathway, distinct from both SKN-1 and the germline, with GST-24 emerging as a critical mediator of the UPS buffering. This research underscores FUdR's role in the UPS modulation and its contribution to survival of worms in low-temperature conditions.

KEYWORDS: floxuridine (FUdR); *C. elegans*; ubiquitin-proteasome system (UPS); detoxification pathway; cold survival

HIGHLIGHTS

- Floxuridine (FUdR) enhances ubiquitin-proteasome system activity in *C. elegans*, independent of primary proteostasis regulators.
- FUdR permits worms to maintain a normal lifespan and facilitates their adaptation to cold in the context of proteasome deficits.

35 • Acting independently of the germline and SKN-1, FUdR triggers a detoxification
36 pathway, with GST-24 as a pivotal component in modulating the ubiquitin-proteasome
37 system.

38 **INTRODUCTION**

39 Maintaining protein homeostasis (proteostasis) is pivotal for cellular health, influencing
40 longevity, metabolism, and stress resistance, as exemplified in notable studies on the nematode
41 *Caenorhabditis elegans* (1, 2, 3). A compromised proteostasis system can lead to premature
42 aging, elevated stress sensitivity, and protein-misfolding diseases (2, 3, 4). A growing body of
43 research highlights that reproductive capacity, influenced by signals from proliferating
44 germline stem cells (GSCs), is a critical regulator of proteostasis, impacting metabolic
45 processes in the soma (5). In nematodes, the GLP-1/Notch signaling pathway is crucial for
46 regulating the GSCs pool and establishing germline polarity; moreover, mutations in GLP-1
47 result in germline loss (6, 7). Remarkably, *glp-1* mutant nematodes exhibit augmented stress
48 resilience, autophagic processes, ubiquitin-proteasome system (UPS) activity, and an extended
49 lifespan. These phenotypic changes are modulated by pivotal molecular regulators, including
50 SKN-1, DAF-12, DAF-16, HSF-1, and TOR (8, 9, 10, 11, 12, 13, 14, 15).

51 Sterility in *C. elegans* can be also chemically induced using floxuridine (FUdR), a well-
52 documented thymidylate synthase inhibitor and anti-cancer agent. FUdR disrupts DNA and
53 RNA synthesis, causing mitotic cell death and inhibition of protein production (16). Given that
54 adult nematode cells are largely post-mitotic, administering FUdR just prior to sexual maturity
55 primarily prevents progeny development without posing a major effect on the adults. While
56 FUdR does not prolong the lifespan of wild-type worms (16), its introduction at the L4 larval
57 stage extends the lifespans of fat-storing *tub-1* and *gas-1* mutants, which exhibit compromised
58 mitochondrial complex functions (17, 18). Interestingly, FUdR-induced sterility in wild-type

59 adult worms significantly enhances their proteostasis, protein folding, and stress responses (19,
60 20, 21, 22). While commonly attributed to its sterilizing capabilities, FUdR has been shown to
61 enhance longevity and proteostasis in nematodes devoid of a germline, suggesting that its
62 beneficial effects are not exclusively linked to reproductive inhibition (22). It is postulated that
63 the mechanism for FUdR proteostasis improvements stems from metabolic shifts or the
64 activation of the DNA damage response pathway (23, 24, 25). Nevertheless, the exact
65 mechanism underlying the proteostasis improvements remains elusive.

66 While proteostasis has traditionally been studied in the context of heat stress, its role
67 under cold has been less explored. Emerging evidence indicates that moderately low
68 temperature (15°C) promote *C. elegans* longevity, enhance proteostasis, and mitigate the
69 accumulation of pathogenic proteins. This protective mechanism is driven predominantly by
70 the PA28γ/PSME-3-activated proteasomes (26). In parallel, Habacher and colleagues, through
71 an RNAi screen, pinpointed PBS-6, a proteasome subunit, as instrumental in cold (4°C)
72 survival (27). This underscores the integral role of the proteasome within the broader
73 proteostasis context during cold adaptation. Building on this foundation, our research sought
74 to discern the relationship between FUdR treatment and its potential role in reinforcing
75 proteostasis, especially when confronting proteasome dysfunction in cold conditions.

76 Our findings highlight that while proteasome dysfunctions impede the nematode's cold
77 (4°C) adaptation, FudR treatment enhances their cold tolerance, bolstering proteasome function
78 even in the absence of its subunits. FudR increases proteasome activity and promotes UPS
79 efficiency independently of well-known proteostasis enhancers like RPN-6.1, HSF-1, and
80 DAF-16 (20, 21, 28), but partially relies on SKN-1 regulated transcription. We also reveal that
81 FUdR activates a detoxification pathway distinct from SKN-1 and the germline, with the GST-
82 24 protein emerging as a crucial factor in this enhanced UPS activity. In conclusion, our

83 investigation provides an advanced understanding of the pathways, both sterility-associated
84 and independent, that are modulated by FUdR.

85 **RESULTS**

86 **Enhancement of proteasome activity via FUdR treatment**

87 To study the impact of FUdR on the *in vivo* UPS activity in *C. elegans,* we utilized a non-
88 cleavable ubiquitin (Ub G76V) fused to a green fluorescent protein (UbV::GFP) under the *sur-*
89 *5* promoter that remains active in most tissues, as a model to assess the functioning of
90 degradation pathway (29). In this system, the ubiquitin moiety of the GFP substrate is poly-
91 ubiquitylated, leading to its recognition and subsequent degradation by the 26S proteasome. In
92 turn, disruption in the UPS activity leads to an increase in UbV-GFP levels, which can be
93 visualized by fluorescence microscopy or western blotting (30, 31) (Fig 1A). Of note, to
94 account for potential variation arising from the transgene expression which might influence the
95 amount of UbV-GFP, worms were also equipped with a mCherry reporter driven by the same
96 *sur-5* promoter (30), and the GFP fluorescent signal was normalized to the mCherry
97 fluorescence.

98 Our reporter strain was exposed to distinct experimental conditions to elucidate the
99 impact of FUdR on the UPS activity. These conditions were designed to impair proteasome
100 function, either via the direct proteasomal inhibition with bortezomib or through RNA
101 interference (RNAi) targeting of proteasome subunits *pas-1* and *pbs-6*, leading to the
102 accumulation of UbV-GFP. Intriguingly, when FUdR treatment was initiated at the young adult
103 stage, we observed a pronounced increase in the UPS activity across all experimental
104 conditions. This proteostasis rescue effect was evidenced by a concomitant reduction in UbV-
105 GFP accumulation, which is attributable to accelerated GFP degradation. Conversely, worms

106 without FUdR treatment manifested a significant accumulation of UbV-GFP owing to
107 compromised proteasome function (Fig 1B).

108 Given that FUdR treatment results in sterility in worms, we examined whether the
109 observed effect was a consequence of FUdR-induced sterility. To this end, worms with RNAi-
110 silenced *pbs-6* were subjected to varying concentrations of FUdR and other pyrimidine analogs
111 (32). Our findings revealed that the beneficial impact of FUdR was confined to concentrations
112 that induced nematode sterility (min. 2 μM; Fig S1A), and a similar enhancement in the UPS
113 performance was also observed with other pyrimidine analogs (Fig S1B).

114 Next, we undertook proteasome activity assays to determine if the observed reduction
115 in UbV-GFP accumulation resulted from elevated proteasome activity. These employed
116 fluorescently labeled probes (28) to measure caspase-like activity (CLA), chymotrypsin-like
117 activity (CTLA), and trypsin-like activity (TLA) in lysates prepared from wild-type worms
118 with or without FUdR treatment. Our data revealed that FUdR was associated with a marked
119 increase in CLA and CTLA activities (Fig 1C). The increase in an activity does not seem to
120 depend on the direct interaction of FUdR with the proteasome, as no changes in the processivity
121 of the recombinant human 26S proteasome were noted in its presence (Fig S1C). To explore
122 the evolutionary conservation of FUdR's impact on proteasome activity, we observed a slight,
123 non-significant increase in activity in HeLa cells with rising FUdR levels, suggesting the full
124 effect of FUdR might necessitate a multicellular mechanism (Fig S1D).

125 Next, we conducted a western blot analysis to evaluate if the heightened UPS activity
126 was attributable to increased proteasome subunit levels. This involved analyzing the levels of
127 PAS-{2, 3, 5, 7} in worms treated with FUdR under proteotoxic stress conditions induced either
128 by the presence of bortezomib or upon silencing *pas-1*, *pbs-2*, *pbs-6*, and *rpn-9* proteasome
129 components. Remarkably, we noted that FUdR treatment resulted in the downregulation of
130 PAS-{2, 3, 5, 7} (Fig 1D). This finding mirrors the observation in germline-less worms, known

131 for enhanced proteostasis and downregulation of 26S subunits (28). For this reason, we checked
132 the translation levels in the FUdR-treated nematodes by employing the surface sensing of
133 translation (SUnSET) method which measures puromycin integration into new proteins. We
134 identified a marked decrease in active translation upon FUdR treatment (Fig S1E), which is
135 probably responsible for the observed decrease in proteasome subunit levels (Fig 1D). This
136 effect is likely tied to germline disruption, as similar reduction was evident in germline-less,
137 temperature-sensitive *glp-1(e2144)* mutant worms (Fig S1E). Thus, despite the reduced
138 synthesis of new proteasome subunits, FUdR-treated worms effectively elevated their
139 proteasome activity.

140 **FUdR bypasses conventional proteostasis regulators**

141 Former studies have underscored the essentiality of a unique proteasome lid subunit, RPN-6.1,
142 in facilitating an upsurge in the UPS activity in sterile *glp-1* mutants (28). Concurrently, sterile
143 worms also necessitate the overexpression of a proteasome core α subunit, PBS-5, to foster
144 proteostasis (9). Because FUdR treatment catalyzes sterility in worms, we conjectured that
145 RPN-6.1 and PBS-5 may be instrumental in the augmentation of proteostasis within FUdR-
146 treated worms.

147 To validate this hypothesis, we conducted similar as described before *in vivo* assays in
148 the reporter strain, examining UbV-GFP accumulation under conditions involving *glp-1* RNAi
149 treatment, either alone or in conjunction with *pbs-5* or *rpn-6.1* RNAi, and with the variable
150 inclusion of FUdR (Fig 2A). Despite *glp-1* RNAi's ability to rescue the UbV-GFP accumulation
151 phenotype under PBS-5 depletion conditions, it could not facilitate UbV-GFP turnover without
152 RPN-6.1. In contrast, FUdR treatment succeeded in augmenting UPS activity by remedying
153 UbV-GFP accumulation across all conditions. Further investigations demonstrated that FUdR's
154 action is not contingent upon any specific proteasome subunit (Fig S2A) nor utilizes autophagy
155 (Fig S2B) to fortify proteostasis. Despite prior assertions that FUdR-mediated resistance to

156 proteotoxic stress is reliant on spermatogenesis (20), our findings suggest that the elevation of
157 UPS activity facilitated by FUdR treatment is not dependent on the spermatogenesis-associated
158 factor, FEM-1 (Fig S2C). This suggests a divergence in the underlying mechanisms responsible
159 for improved proteostasis between *glp-1* dysfunction-induced sterile worms and those rendered
160 sterile by FUdR treatment.

161 To discern the factors essential for UPS activity improvement via FUdR treatment, we
162 induced silencing of *daf-16*, *hsf-1*, *pqm-1*, and *skn-1* factors recognized to regulate proteostasis
163 and confer protection against proteotoxic stress (8, 14, 15, 21, 28), in the presence of
164 bortezomib. FUdR treatment successfully corrected the UbV-GFP accumulation phenotype in
165 cells devoid of HSF-1, DAF-16, and PQM-1. Conversely, the rescue of UbV-GFP
166 accumulation was not completely achieved under *skn-1* RNAi conditions (Fig 2B). This
167 observation aligns with previous research that revealed FUdR-mediated protection against
168 proteotoxic stress independent of *hsf-1* and *daf-16* transcription factors (20).

169 To corroborate the significance of *skn-1* in the enhancement of UPS activity, we
170 executed a similar as previously described proteasome activity assay, using lysates prepared
171 from wild-type worms under *skn-1* RNAi conditions, with or without FUdR. Our data unveiled
172 that in the absence of SKN-1, worms did not exhibit elevated proteasome activity, even when
173 FUdR was present (Fig S2D). Together, our results outline a mechanistic divergence in
174 enhancing proteostasis in FUdR-treated and sterile *glp-1 C. elegans*, revealing that the effects
175 of FUdR partially rely on SKN-1.

176 **FUdR prolongs lifespan and promotes cold survival under proteasome deficiencies**

177 The successful induction of hibernation in *C. elegans* under cold conditions is contingent on a
178 β subunit of the proteasome, PBS-6 (27). Also, prior studies have underscored the
179 indispensability of proteasome components for the longevity of worms (33). In the light of our
180 results that highlight FUdR's capacity to amplify proteasome activity despite its deficits, we

181 conducted cold-survival and lifespan assays (Fig 3A) on wild-type *C. elegans,* with
182 simultaneous RNAi depletion of PAS-1, PBS-2, or PBS-6 proteasome subunits. Our data
183 delineated that FUdR treatment notably increased the lifespan of worms subjected to
184 proteasome disruption (Fig 3B, Fig S3A). Additionally, we discovered that FUdR treatment
185 could effectively re-establish the survival of worms in cold survival assay, even amid
186 proteotoxic stress induced by the depletion of PAS-1, PBS-2, PBS-6, and RPN-9 (Fig 3C).
187 Notably, during cold survival assay, *C. elegans* requires a brief adaptation period at 10ºC before
188 exposure to cold incubation at 4ºC. The absence of this adaptation period, followed by an abrupt
189 cold incubation for 24 hr or more, has been proven lethal for the worms (34). Hence, we
190 conducted the cold survival assay with or without the adaptation period in the presence of
191 FUdR, under proteasome malfunction caused by knockdown of PBS-6. The FUdR treatment
192 significantly increased worm survival upon sudden cold shock (without an adaptation period),
193 even under compromised proteasome function (Fig S3B).

194 To scrutinize the impact of tissue-specific proteostasis collapse on cold survival, we
195 silenced *pbs-6* in wild-type strains and strains permitting tissue-specific RNAi depletion in
196 muscles, intestines, germline, or neurons, again with or without FUdR. Our findings revealed
197 that the knockdown of PBS-6 in neurons and intestines had the most pronounced impact on
198 cold survival, which can be fully rescued by the FUdR treatment (Fig S3C).

199 Subsequently, we posited that FUdR-induced sterility plays a role in enhancing cold
200 survival, a hypothesis supported by experiments involving both *glp-1(e2144)* sterile mutants
201 and wild-type worms. The cold survival assay indicated enhanced survival in *glp-1(e2144)*
202 mutants compared to wild-type worms when PBS-6 was depleted (Fig 3D). Moreover, this
203 survival advantage of *glp-1(e2144)* worms was further potentiated in the presence of FUdR,
204 suggesting that the mechanisms of cold tolerance induced by FUdR are likely distinct from the
205 protective effects conferred by sterility alone.

206 As previously demonstrated, the SKN-1 transcription factor is partially required for
207 FUdR to fully restore the enhanced proteostasis phenotype (Fig 2B). Therefore, we executed a
208 cold survival assay involving both wild-type and *skn-1(mg570)* loss of function mutants, with
209 or without RNAi silencing of *pbs-6* and FUdR. While the *skn-1(mg570)* worms exhibited no
210 notable decline in survival after cold incubation in the control RNAi condition, a significant
211 reduction in survival was noted for *skn-1(mg570)* mutants when subjected to proteasome
212 dysfunction by *pbs-6* silencing and cold exposure (Fig 3E). The observed decline was, albeit
213 not entirely, rescued by FUdR treatment.

214 **FUdR induces a detoxification pathway buffering UPS during proteasome inhibition**

215 Based on our findings from the SUnSET assay (Fig. S1E), we speculated that the suppressive
216 action of FUdR on translation could play a significant role in supporting UPS activity, given
217 the well-established challenge that newly produced proteins pose to the proteostasis machinery
218 (35, 36, 37, 38). However, despite the pronounced FUdR-mediated reduction in new protein
219 synthesis in *skn-1(mg577)* mutant worms (Fig 4A), the role of the SKN-1 transcription factor
220 remains significant for FUdR's ability to promote UPS function when confronted with
221 proteasome inhibitors like bortezomib (Fig 2B). Furthermore, our findings show that while
222 both FUdR and the *glp-1(e2144)* mutation significantly reduce translation, FUdR distinctively
223 triggers UPS-enhancing mechanisms in germline-less *glp-1* mutants, evident in its ability to
224 circumvent the requirement for RPN-6.1 (Fig 2A). Prior research has demonstrated that in
225 response to global translation inhibition, ribosome availability facilitates selective translation,
226 especially of stress response factors (37, 38, 39, 40). Given these insights, we hypothesized
227 that the mechanism underlying FUdR's action could be centered on the selective translation of
228 the UPS buffering proteins, which should also occur in *glp-1* and *skn-1* mutants. To investigate
229 this, we conducted a targeted proteomic analysis of adult wild-type, *glp-1(e2144)*, and *skn-*
230 *1(mg570)* worms treated with 400 μM FUdR, aiming to identify proteins whose level is

231 uniquely increased by FUdR. We identified and consistently quantified 5855 protein groups
232 across all experimental conditions and three independent biological replicates. The analysis
233 revealed that the FUdR treatment affected total levels of numerous proteins (717 up- and 821
234 down-regulated in wild-type, 416 up- and 442 down-regulated in *glp-1(e2144)*, 1132 up- and
235 1061 down-regulated in *skn-1(mg570)* worms) (Table S1).

236 To uncover pathways activated solely by FUdR, we manually categorized functions of
237 proteins up-regulated across all three strains upon FUdR treatment (Table S2, Fig S4A). Our
238 analysis revealed that over 33% of these proteins are implicated in detoxification and innate
239 immunity pathways (Fig 4B), indicating that FUdR induces a detoxification response that is
240 autonomous of both germline and *skn-1*. To eliminate the possibility that this induction is due
241 to metabolites produced by bacterial metabolism of FUdR or bacterial infection, we examined
242 UbV-GFP reporter degradation in worms fed with both live and killed HT115 *Escherichia coli*,
243 in the presence or absence of bortezomib and FUdR. Our results demonstrated that FUdR
244 effectively mitigated UbV-GFP accumulation under both bacterial conditions (Fig S4B).

245 To further elucidate our proteomic findings and clarify if detoxification proteins are
246 involved in FUdR-mediated proteostasis enhancement, we focused on RNAi-mediated
247 depletion of the most abundant detoxifying proteins - specifically GST-24, UGT-39, UGT-48,
248 CYP-35A3, and CYP-14A5 - that were uniquely upregulated under FUdR treatment, while
249 monitoring the turnover of the UBV-GFP reporter. Our data showed that GST-24 and CYP-
250 14A5, when depleted individually, can affect UPS activity (Fig S4C). Notably, FUdR
251 effectively reinstates proteasomal degradation in worms where SKN-1 is silenced alone or
252 combined with UGT-39, UGT-48, CYP-35A3, or CYP14A5 (Fig 4C). This restorative effect
253 is not observed when GST-24 is co-depleted with SKN-1 (Fig 4C), highlighting crucial role of
254 GST-24 in the detoxification pathway that contributes to FUdR's enhancement of the UPS.
255 However, the singular RNAi depletion of GST-24 from the array of FUdR-upregulated

256 detoxifying proteins did not compromise the safeguarding effect of FUdR on the worms'
257 resistance to low temperatures upon PBS-6 depletion (Fig S4D), indicating the cumulative
258 action of other mechanisms.

259 A previous study has suggested that dopamine signaling induces the xenobiotic stress
260 response and improves proteostasis (41). To validate whether the neuronal signal is essential
261 in improving the UPS activity upon FUdR induction, we measured the turnover of UbV-GFP
262 reporter upon depleting the sensory neuron ciliary components CHE-12 and CHE-13 (42, 43)
263 with or without knockdown of SKN-1. Our findings indicate that individual silencing of either
264 *che-12* or *che-13* exerts no discernible impact on UPS activity (Fig S4E). Upon simultaneous
265 silencing of SKN1 and either CHE-12 or CHE-13, we noticed an alteration in proteostasis,
266 further emphasized by FUdR's inability to fully ameliorate UbV-GFP degradation when CHE-
267 12 or CHE-13 was explicitly targeted (Fig S4E). This suggests the involvement of neuronal
268 signaling in the regulation of proteostasis by FUdR.

269 **DISCUSSION**

270 While FUdR is primarily known for inducing reproductive arrest, it also exerts secondary
271 effects on various facets of *C. elegans* physiology, such as proteostasis and stress response
272 mechanisms (16, 19, 20, 21, 22). Our data indicate that FUdR augments the proteasome's
273 caspase-like and chymotrypsin-like activities, akin to the effects observed in the sterile *glp-*
274 *1(e2144)* mutant (28). Although both FUdR and germline-deficient worms are known to
275 elevate proteasome activity and stress resistance (13, 22), FUdR appears to act independently
276 of germline signaling. Enhanced proteostasis in *glp-1* mutants is contingent upon RPN-6.1, a
277 lid subunit of the 26S proteasome (28), whereas the effect of FUdR is not. Moreover, these
278 mechanisms further diverge: while *glp-1* mutants are dependent on *daf-16* for both lifespan

279 extension and elevated proteasome activity (28), the enhancement of UPS activity in FUdR-
280 treated worms is partially attributable to the *skn-1* transcription factor, but not *daf-16*.
281 Our findings demonstrate that FUdR treatment initiates a xenobiotic detoxification
282 pathway involving innate immune response proteins independently of SKN-1 and germline
283 signaling. Although SKN-1 generally activates proteasome subunits and is influenced by lipids
284 in sterile animals (14, 44), FUdR does not rely on specific 26S proteasome subunits or
285 autophagy for its effects. Instead, SKN-1 appears to have an alternative role in enhancing UPS
286 activity in the presence of FUdR, possibly through SKN-1-dependent and independent
287 xenobiotic pathways (45, 46, 47). We note that the latter is involved in the up-regulation of i.a.,
288 GST-24, previously linked to stress resistance in *C. elegans* (48). Furthermore, given that
289 FUdR induces DNA breaks, activating damage repair pathways (24), and that DNA breaks in
290 the germline improve UPS activity through an innate immune response (49), it is plausible that
291 FUdR triggers this detoxification pathway in response to DNA damage. Parallelly, we observed
292 that treatment with FUdR enhances the ability of *C. elegans* to withstand cold stress at 4ºC,
293 even bypassing the usual need for a preparatory acclimatization phase at 10ºC. This raises the
294 possibility that FUdR treatment mimics or induces adaptive processes normally activated
295 during this acclimatization period. Previous research has shown that moderate cold exposure
296 at 10ºC triggers shifts in lipid metabolism, which are likely crucial for enhanced cold resistance
297 (50, 51). Interestingly, lipid metabolism in *C. elegans* is deeply interwoven with innate immune
298 responses; specific fatty acids and their synthesizing enzymes are essential for immune gene
299 expression and pathogen resistance (52). Given that FUdR pre-treatment activates
300 detoxification pathways in the worms prior to exposure to severe cold, it is conceivable that
301 such pathways and lipid metabolism may interact to confer cold resilience.
302 It is noteworthy that the beneficial effects of FUdR in promoting worms survival and
303 protein turnover are not dependent on evolutionarily preserved transcriptional regulators DAF-

304 16 and PQM-1, recognized for their cooperative role in enhancing resilience to cold conditions
305 through the upregulation of FTN-1/ferritin (53). This delineates a distinct mechanistic route
306 through which FUdR modulates cellular homeostasis and also raises intriguing questions about
307 the potential cross-talk between various stress response pathways and how they might be
308 selectively activated or bypassed.

309 Our study offers a comprehensive analysis of the diverse functional roles of FUdR in
310 *C. elegans*, emphasizing its modulation of the UPS efficiency, detoxification pathways, and
311 cold resilience mechanisms. Although there are marked differences in the architecture of
312 immune systems between nematodes and higher organisms, several innate immunity and
313 detoxification mechanisms are evolutionarily preserved, suggesting potential translational
314 relevance (54). These findings thus warrant further exploration of the influence of FUdR on
315 proteasomal activity, particularly in the context of its co-administration with agents like
316 bortezomib in oncological patients (55, 56). Additionally, it would be valuable to study whether
317 FUdR or related molecules have the potential to enhance cellular resilience in mammals
318 subjected to environmental stressors, including temperature fluctuations. Such research could
319 extend our grasp of the adaptability-promoting properties of these compounds across different
320 species.

321

322 **MATERIALS AND METHODS**

323 **Worm maintenance**

324 *C. elegans* were cultured on nematode growth medium (NGM) plates seeded with OP50 or
325 HT115 *E. coli* strains. These culture conditions were maintained at various temperatures,
326 namely 16°C, 20°C, or 25°C, depending on both the worm strain and the specific requirements
327 of the experimental protocol, following standard *C. elegans* culture techniques (57). Dead
328 bacterial food sources were prepared by exposing bacterial cultures to paraformaldehyde (58).
329 Worm strains utilized for different experimental setups are cataloged in Table 1. Unless stated
330 otherwise, NGM plates were supplemented with 400 μM of floxuridine (FUdR; Cat: F0503;
331 Sigma Aldrich). In some instances, other pyrimidine analogs were employed, including 5-
332 fluorocytosine (FC; Cat: 543020; Sigma Aldrich), 5-fluorouracil (FU; Cat: F6627; Sigma
333 Aldrich), and 5-fluoro-2′-deoxycytidine (FCdR; Cat: F5307; Sigma Aldrich), as well as
334 proteasome inhibitor bortezomib (Cat: 504314; Sigma Aldrich), each at a concentration of 10
335 μM.

336 **Table 1.** *C. elegans* strains used in this study.

Strain	Source	Purpose
C. elegans: Bristol (N2)	CGC[1]	Wild-type; control worms
skn-1(mg570)	CGC	*skn-1* mutant
glp-1(e2144)	CGC	*glp-1* mutant
hhls72*[unc-119(+); sur-5::mCherry]*, hhls64*[unc-119(+); sur-5::UbiV-GFP]*	(30)	UPS activity reporter
rde-1(mkc36); mkcSi13	(59)	Germline-specific RNAi
rde-1(ne219); kzls20	(60)	Body wall muscle-specific RNAi

rde-1(ne219); kbls7	(61)	Intestine-specific RNAi
TU3311 *[uls60 (unc-119p::YFP + unc-119p::sid-1)]*	(62)	Neuron-specific RNAi

337 [1] Caenorhabditis Genetics Center

338 **RNA interference**

339 Gene silencing was carried out by the standard RNAi feeding method using clones from the
340 Ahringer *C. elegans* RNAi library (63). RNAi was applied at different stages for each target
341 gene, as described in Table S3. NGM plates supplemented with 1 mM IPTG (Cat: IPT001;
342 BioShop) and 25 µg/µl carbenicillin (Art. No. 6344.2; Carl Roth Gmbh & Co.) were seeded
343 with bacteria expressing double-stranded RNA from L4440 plasmid; *E. coli* HT115 (DE3)
344 bacteria containing empty L4440 plasmid were used as control.

345 **Lifespan assay**

346 Synchronized late-stage L4 worms were silenced for *pbs-6*, *pas-1*, *pbs-2,* or control RNAi
347 (empty vector) for 40 hr with or without FUdR. Subsequently, lifespan measurements were
348 carried out at a constant temperature of 20°C. Approximately 30 nematodes were maintained
349 on each 6 cm diameter agar plate for the duration of the lifespan assay. Daily evaluations were
350 performed to monitor the worms for movement and pharyngeal pumping as vitality indicators.
351 Worms were deemed to have reached the end of their lifespan if they failed to display these
352 physiological activities. Any animals manifesting bagging phenotypes or found to have
353 crawled off the agar surface were censored. Data was analyzed using the Log-Rank (Mantel-
354 Cox) test in the GraphPad Prism 9 software. The experiments were not randomized. No
355 statistical methods were used to predetermine the sample size. The investigators were blinded
356 to allocation during experiments.

357

358

359 **Cold survival assay**

360 To assess the impact of specific gene knockdown and FUdR treatment on cold tolerance,
361 approximately 30 late-stage L4 *C. elegans* were subjected to gene silencing. The gene silencing
362 was performed for 40 hr at a controlled temperature of 20°C, in the presence or absence of
363 FUdR, according to protocols detailed in the study by Habacher and colleagues (27).

364 **Adaptation and exposure to cold conditions:** Following the gene silencing phase, the
365 nematodes were acclimatized to a moderately cold environment at 10°C for 6 hr. Subsequently,
366 the worms were exposed to a colder temperature setting at 4°C and maintained at this condition
367 for 72 hr.

368 **Recovery and scoring:** After the 3-day cold exposure, the worms were allowed to recover at
369 20°C, lasting between 3 and 4 hr. Following the recovery phase, an assessment was carried out
370 to distinguish between live and dead specimens.

371 **Cold incubation treatment:** As a control, cold incubation was administered by directly
372 transferring the worms from a 20°C environment to a 4°C setting for 72 hr without prior
373 acclimatization.

374 **UbV-GFP substrate turnover assay**

375 To explore the turnover dynamics of the ubiquitin-based substrate in the presence of gene
376 knockdown and various pharmacological treatments, we utilized L4 stage hermaphrodites of
377 two specific strains: hhls72*[unc-119(+); sur-5::mCherry]* and hhls64*[unc-119(+); sur-*
378 *5::UbiV-GFP]*. Nematodes were silenced for the target genes over 40 hr at a consistent
379 temperature of 20°C. During this gene-silencing stage, the worms were treated with varying
380 concentration of FUdR, FU, FC, FCdR, and 100 nM bortezomib. Post-treatment, nematodes
381 were subjected to fluorescence imaging employing an Axio Zoom.V16 microscope outfitted

382 with an Axiocam 705 monochrome CMOS camera (Carl Zeiss). Images were captured across
383 brightfield, green, and red channels. Subsequent data processing was performed using the
384 AxioVision 4.7 analysis software (Carl Zeiss) to quantify the rates of substrate turnover, as
385 reflected by the intensity and distribution of fluorescence signals.

386 **Proteasome activity measurement in worms**

387 Approximately 7000 L4 stage worms were silenced for the respective genes at a concentration
388 of 400 µM for 40 hr at 20°C. Next, worms were harvested and lysed in 50 mM Tris-HCl,
389 250 mM sucrose, 5 mM $MgCl_2$, 0.5 mM EDTA, 2 mM ATP, and 1 mM dithiothreitol at pH 7.5.
390 Bortezomib was introduced to the lysate as a control at a concentration of 20 nM. The caspase-
391 like, chymotrypsin-like, and trypsin-like activities of the proteasome were subsequently
392 measured following the methods described (28). Proteasome activity was also measured using
393 5 nM of recombinant human 26S proteasome (Cat: E-365; R&D Systems).

394 **Proteasome activity measurement in cells**

395 HeLa Flp-In T-Rex cell line (a kind gift from R. Szczęsny) was cultured in Dulbecco's
396 Modified Eagle's Medium (Cat: 6429; Sigma Aldrich) supplemented with 10% fetal bovine
397 serum (Cat: F9965; Sigma Aldrich) and 1% Antibiotic-Antimycotic (Cat: 15240096; Gibco) at
398 37°C with 5% CO_2 in a humidified incubator. HeLa cells were seeded in black 96-well tissue
399 culture plates (Cat: 655090; Greiner) at a density of 20,000 cells in a total volume of 100 µl
400 per well. The next day, the cells were subjected to a 6-hr treatment with FUdR at 2.5 µg/ml
401 concentration in the growing media. Where indicated, the cells were also treated with 10 nM
402 bortezomib (Cat: 504314; Merck). The control cells received dimethyl sulfoxide. Using the
403 Proteasome 20S Activity Assay Kit (Cat: MAK172; Sigma Aldrich), 10.75 µl of LLVY-R110
404 Substrate was mixed with 4300 µl of the Assay Solution to create the Proteasome Assay
405 Loading Solution, according to the manufacturer's guidelines. Subsequently, 100 µl of this

406 prepared solution was accurately pipetted into each assay plate well. The plate was then
407 incubated at 37°C for 2 hr. After the incubation period, the fluorescence intensity (λ_{ex} = 490
408 nm, λ_{em} = 525 nm) was gauged using the TECAN Infinite 200 Pro plate reader equipped with
409 the Magellan Pro software to ascertain proteasome activity.

410 **Surface sensing of translation assay**

411 The surface sensing of translation (SUnSET) assay was employed to evaluate protein synthesis
412 rates, following the delineated methodology (64). A minimum of 7,000 worms were incubated
413 in 4 mL of S-complete liquid media supplemented with 750 µL of 10X *E. coli* food, engineered
414 to express double-stranded RNA against targeted genes, and 0.5 mg/mL puromycin (Cat: ant-
415 pr-1; Invivogen). The incubation occurred at 20°C with a consistent shaking speed of 200 rpm
416 for 5 hr. The worms were then harvested, washed three times in M9 buffer, and subsequently
417 lysed in a lysis buffer (50 mM KCl, 10 mM Tris-HCl pH 8.2, 2.5 mM $MgCl_2$, 0.07% NP-40,
418 0.7% Tween-20, 0.1% gelatin), supplemented with protease inhibitor (Cat: 04693159001;
419 Roche). Protein concentration was determined using the Pierce Rapid Gold BCA Protein Assay
420 Kit (Cat: A53225; Thermo Fisher Scientific) and western blotting.

421 **Western blotting**

422 Proteins were separated by electrophoresis on 12% acrylamide gels using a running buffer
423 containing 25 mM Tris, 190 mM glycine, and 0.1% SDS. Electrophoresis was conducted at a
424 constant voltage of 150 V. Subsequently, protein samples were transferred to PVDF
425 membranes through a wet transfer method at 100 V for one hour. The transfer buffer contained
426 25 mM Tris, 190 mM glycine, and 10% methanol, with a pH of 8.3. For protein visualization,
427 the membranes were treated with Invitrogen No-Stain Protein Labeling Reagent (Cat: A44717;
428 Thermo Scientific) according to the manufacturer's guidelines. Following this, the membranes

429 were blocked in a solution of 5% skimmed milk dissolved in TBST buffer (50 mM Tris, 150
430 mM NaCl, 0.1% Tween 20, pH 7.5) for 45 min at room temperature. Primary antibody
431 incubation was performed overnight at 4°C using either anti-GFP antibody (Cat: GF208R;
432 Thermo Fisher Scientific), anti-PAS-7 antibody (Cat: CePAS7; Developmental Studies
433 Hybridoma Bank (DSHB)), anti-proteasome 20S alpha 1+2+3+5+6+7 antibody (Cat: ab22674;
434 Abcam) or anti-puromycin (Cat: MABE343; Merck), both prepared in 5% skimmed milk in
435 TBST buffer. Post-incubation, membranes were washed three times with TBST for 10 min
436 each and incubated with the appropriate secondary antibodies, prepared in the blocking
437 solution, for 45 min at room temperature. Membranes were subsequently developed and
438 visualized using a ChemiDoc Imaging System from Bio-Rad.

439 **Proteomics analysis**

440 *C. elegans* were extracted using the Sample Preparation by Easy Extraction and Digestion
441 (SPEED) protocol (65). In brief, *C. elegans* were solubilized in concentrated Trifluoroacetic
442 Acid (TFA; Cat: T6508; Sigma Aldrich) (cell pellet/TFA 1:2-1:4 (v/v)) and incubated for 2-10
443 min at room temperature. Next, samples were neutralized with 2 M Tris-Base buffer using 10x
444 volume of TFA and further incubated at 95°C for 5 min after adding Tris(2-
445 carboxyethyl)phosphine (final concentration 10 mM) and 2-chloroacetamide (final
446 concentration 40 mM). Turbidity measurements determined protein concentrations at 360 nm,
447 adjusted to the same concentration using a sample dilution buffer (2M TrisBase/TFA 10:1
448 (v/v)), and then diluted 1:4-1:5 with water. Digestion was carried out overnight at 37°C using
449 trypsin at a protein/enzyme ratio of 100:1. TFA was added to a final concentration of 2% to
450 stop digestion. The resulting peptides were labeled using an on-column TMT labeling protocol
451 (66). TMT-labeled samples were compiled into a single TMT sample and concentrated.
452 Peptides in the compiled sample were fractionated (8 fractions) using the Pierce High pH

453 Reversed-Phase Peptide Fractionation Kit (Cat: 84868; Thermo Fisher Scientific). Prior to
454 liquid chromatography–mass spectrometry (LC-MS) measurement, the peptide fractions were
455 reconstituted in 0.1% TFA, 2% acetonitrile in water. Chromatographic separation was
456 performed on an Easy-Spray Acclaim PepMap column 50 cm long × 75 µm inner diameter
457 (Cat: PN ES903; Thermo Fisher Scientific) at 55°C by applying 120 min acetonitrile gradients
458 in 0.1% aqueous formic acid at a flow rate of 300 nl/min. An UltiMate 3000 nano-LC system
459 was coupled to a Q Exactive HF-X mass spectrometer via an easy-spray source (all Thermo
460 Fisher Scientific). The Q Exactive HF-X was operated in TMT mode with survey scans
461 acquired at a resolution of 60,000 at m/z 200. Up to 15 of the most abundant isotope patterns
462 with charges 2-5 from the survey scan were selected with an isolation window of 0.7 m/z and
463 fragmented by higher-energy collision dissociation (HCD) with normalized collision energies
464 of 32, while the dynamic exclusion was set to 35 s. The maximum ion injection times for the
465 survey and tandem mass spectrometry (MS/MS) scans (acquired with a resolution of 45,000 at
466 m/z 200) were 50 and 96 ms, respectively. The ion target value for MS was set to 3e6 and for
467 MS/MS to 1e5, and the minimum AGC target was set to 1e3.

468 The data were processed with MaxQuant v. 1.6.17.0 (67), and the peptides were
469 identified from the MS/MS spectra searched against Uniprot *C. elegans* reference proteome
470 (UP000001940) using the built-in Andromeda search engine. Raw files from the liquid
471 chromatography with tandem mass spectrometry (LC-MS/MS) measurements of 8 tryptic
472 peptide fractions were analyzed together. Reporter ion MS2-based quantification was applied
473 with reporter mass tolerance = 0.003 Da and min. reporter PIF = 0.75. Cysteine
474 carbamidomethylation was set as a fixed modification, and methionine oxidation,
475 glutamine/asparagine deamination, and protein N-terminal acetylation were set as variable
476 modifications. For *in silico* digests of the reference proteome, cleavages of arginine or lysine
477 followed by any amino acid were allowed (trypsin/P), and up to two missed cleavages were

allowed. The false discovery rate (FDR) was set to 0.01 for peptides, proteins, and sites. A match between runs was enabled. Other parameters were used as pre-set in the software. Unique and razor peptides were used for quantification, enabling protein grouping (razor peptides are the peptides uniquely assigned to protein groups and not to individual proteins). Reporter intensity corrected values for protein groups were loaded into Perseus v. 1.6.10.0. (68). Standard filtering steps were applied to clean up the dataset: reverse (matched to decoy database), only identified by site, and potential contaminant (from a list of commonly occurring contaminants included in MaxQuant) protein groups were removed. Reporter intensity corrected values were log2 transformed, and protein groups with all values were kept. Reporter intensity values were then normalized by median subtraction within TMT channels. Student's t-tests (permutation-based FDR = 0.001, S0 = 0.1) were performed on the dataset to return protein groups, whose levels were statistically significantly changed between the sample groups investigated.

DATA AVAILABILITY

The proteomics data was uploaded to the ProteomeXchange Consortium (69) via the PRIDE partner repository (70) with the dataset identifier PXD045805. The datasets used and/or analyzed during the current study are available from the corresponding author upon reasonable request.

COMPETING INTERESTS

The authors declare no competing interests.

AUTHOR CONTRIBUTIONS

AAD: Data curation; conceptualization; formal analysis; investigation; visualization; writing. **NAS**: Data curation; formal analysis; visualization; writing. **MP**: Investigation. **RAS**: Investigation (proteomics). **WP**: Conceptualization; resources; supervision; funding

502 acquisition; validation; project administration; writing. All authors read and approved the
503 manuscript.

504 **ACKNOWLEDGMENTS**

505 Proteomic measurements were performed at the Proteomics Core Facility, IMol Polish
506 Academy of Sciences. Special thanks to Dorota Stadnik for help with sample preparation and
507 LC-MS/MS measurements. We thank the Caenorhabditis Genetics Center (funded by the NIH
508 National Center for Research Resources, P40 OD010440) for *C. elegans* strains. We thank
509 Roman Szczęsny for the HeLa Flp-In T-Rex cell line. We also acknowledge Marta Niklewicz
510 and Karolina Milcz for their technical assistance and Rafał Ciosk for comments on the
511 manuscript.

512 **FUNDING**

513 The Norwegian Financial Mechanism 2014–2021 and operated by the Polish National Science
514 Centre, Poland (under the project contract number 2019/34/H/NZ3/00691).

515 **FIGURES' LEGENDS**

516 **Figure 1. Enhancement of proteasome activity by FUdR. (A)** A scheme illustrating the
517 method for monitoring *in vivo* UPS activity, employing UbV-GFP as the indicative reporter.
518 **(B)** *In vivo* UPS activity assay showing the effect of FUdR on UbV-GFP turnover in the
519 presence of the proteasome inhibitor bortezomib (Btz) and during the RNAi depletion of *pas-*
520 *1* and *pbs-6* proteasome subunits. Scale bar corresponds to 400 µm. **(C)** FUdR's effect on
521 proteasome activity, as measured by trypsin-like, chymotrypsin-like, and caspase-like activity
522 in wild-type worms with or without FUdR treatment. Bortezomib (Btz) served as the negative
523 control. Proteasome activity is represented as slopes obtained from kinetic measurements. The
524 experiments were conducted thrice as separate biological replicates, and significance levels (**

525 - $P \leq 0.01$) were determined using an unpaired t-test with Welch's correction. **(D)** Western blot
526 showing levels of PAS-2, PAS-3, PAS-5, and PAS-7 proteasome subunits levels in wild-type
527 worms following the RNAi depletion of RPN-9, PBS-6, PBS-2 and PAS-1 proteasome
528 components in the presence or absence of FUdR, as depicted by using anti-proteasome 20S
529 alpha 1+2+3+5+6+7 antibody. The No-Stain Protein Labeling Reagent was used to confirm
530 equal protein loading.

531 **Figure 2. The improved UPS activity mediated by FUdR partially relies on *skn-1*. (A)** *In*
532 *vivo* UPS activity assay showing the effect of FUdR on UbV-GFP turnover in worms subjected
533 to *glp-1*, *pbs-5* and *rpn-6.1* RNAi silencing, with or without FUdR. **(B)** *In vivo* UPS activity
534 assay showing the effect of FUdR on UbV-GFP turnover in worms subjected to *hsf-1*, *daf-16*,
535 *pqm-1*, and *skn-1* RNAi silencing in the absence or presence of bortezomib (Btz). In panels A
536 and B, the scale bar corresponds to 400 μm.

537 **Figure 3. FUdR enhances lifespan and cold survival upon proteasome deficits. (A)** A
538 schematic representation of cold survival and lifespan assays. **(B)** The lifespan of wild-type
539 worms when exposed to control or *pbs-6* RNAi in the presence or absence FUdR. Number of
540 worms used in the study: control RNAi: n=123 (+ FUdR) or n=139 (- FUdR); *pbs-6* RNAi:
541 n=129 (+ FUdR) or n=149 (- FUdR). **(C)** The impact of FUdR on the cold survival rate of wild-
542 type worms during the knockdown of PAS-1, PBS-2, PBS-6, and RPN-9, considering both
543 FUdR-treated and untreated conditions. Data was analyzed using two-way ANOVA and the
544 significance levels obtained from the Šidák's multiple comparisons test are indicated for the
545 compared conditions (ns - not significant, * - $P \leq 0.05$, ** - $P \leq 0.01$, *** - $P \leq 0.001$, **** -
546 $P \leq 0.0001$). **(D)** The impact of FUdR on the cold survival of wild-type and *glp-1(e2144)*
547 worms subjected to control and *pbs-6* RNAi. Data was analyzed using two-way ANOVA and
548 the significance levels obtained from the Šidák's multiple comparisons test are indicated for

549 the compared conditions (ns - not significant, ** - $P \leq 0.01$, **** - $P \leq 0.0001$). **(E)** The impact
550 of FUdR on the cold survival of wild-type and *skn-1(mg570)* worms subjected to control and
551 *pbs-6* RNAi. Data was analyzed using two-way ANOVA and the significance levels obtained
552 from the Tukey's multiple comparisons test are indicated for the compared conditions (ns - not
553 significant, *** - $P \leq 0.001$, **** - $P \leq 0.0001$). In panels C-E, at least 90 animals were scored in
554 three independent biological replicates.

555 **Figure 4. FUdR promotes detoxification pathway independent of *skn-1* and *glp-1*. (A)**
556 Western blot showing global translation activity in wild-type, *glp-1(e2144)*, and *skn-1(mg570)*
557 worms, in the presence or absence of FUdR, as depicted by using anti-puromycin antibody.
558 The No-Stain Protein Labeling Reagent was used to confirm equal protein loading. **(B)** Pie
559 chart representing the functional categories of proteins from our proteomics study that
560 exhibited a marked increase (fold change > 1.0), observed consistently in wild-type, *glp-*
561 *1(e2144)*, and *skn-1(mg570)* worms specifically due to FUdR treatment. The significance of
562 proteomic findings was confirmed through student's t-tests, setting a *P*-value threshold < 0.05
563 while maintaining the false discovery rate under 0.01. Functional annotations were compiled
564 by manual review. **(C)** *In vivo* UPS activity assay showing the effect of FUdR on UbV-GFP
565 turnover in worms subjected to *skn-1* RNAi silencing alone or in combination with *gst-24*, *ugt-*
566 *39*, *ugt-48*, *cyp35A3*, and *cyp14A5* RNAi silencing, with or without FUdR. Scale bar
567 corresponds to 400 µm.

568 **SUPPLEMENTARY TABLES' AND FIGURES' LEGENDS**

569 **Table S1**. Results of proteomics analysis showing changes in protein abundance in wild-type,
570 *glp-1(e2144)*, and *skn-1(mg570)* worms in the presence or absence of FUdR.

571 **Table S2**. Proteins up-regulated in wild-type, *glp-1(e2144)*, and *skn-1(mg570)* upon FUdR
572 treatment with manually categorized functions.

573 **Table S3**. Worm stages designated for specific RNAi treatments.

574 **Figure S1**. **Pyrimidine analogs improve UPS activity. (A)** *In vivo* UPS activity assay
575 showing the effect of different concentrations of FUdR on UbV-GFP turnover. **(B)** *In vivo* UPS
576 activity assay showing the effect of different pyrimidine analogs, 5-fluorouracil (FU), 5-
577 fluorocytosine (FC), and 5-fluorodeoxycytidine (FCdR), on UbV-GFP turnover. In panels A
578 and B, the scale bar corresponds to 400 μm. **(C)** Effect of different concentrations of FUdR on
579 the activity of purified human 26S proteasome in HeLa cells, as measured by trypsin-like,
580 chymotrypsin-like, and caspase-like activity in wild-type worms with or without FUdR
581 treatment. Bortezomib (Btz) served as the negative control. Proteasome activity is represented
582 as slopes obtained from kinetic measurements. The experiments were conducted thrice as
583 separate biological replicates. **(D)** FUdR effect on chymotrypsin-like proteasome activity in
584 HeLa cells. Cells were treated with final concentrations of 0.4 and 2 μM of FUdR and 10 nM
585 bortezomib (Btz) as control for 6 hr. The assay was conducted by incubating the cells with 100
586 μl Proteasome Assay Loading Solution for 2 h as described in the methods. Results from three
587 technical replicates were corrected for background by subtracting the fluorescence of the
588 medium without cells and further normalized to dimethyl sulfoxide control. The graph shows
589 the average values obtained from either two or four biological replicates for experiments that
590 involve FUdR or Btz, respectively. **(E)** Western blot showing global translation activity in
591 wild-type and *glp-1(e2144)* worms, in the presence or absence of FUdR, as depicted by using
592 the anti-puromycin antibody. The No-Stain Protein Labeling Reagent was used to confirm
593 equal protein loading.

594 **Figure S2. FUdR buffers UPS activity under proteasome-compromised conditions. (A)**
595 Western blot showing the impact of FUdR on UbV-GFP reporter turnover upon depletion of
596 various 26S subunits in control worms, as depicted by using anti-GFP antibody. The No-Stain

597 Protein Labeling Reagent was used to confirm equal protein loading. **(B)** Western blot showing
598 degradation of UbV-GFP in control, *atg-1* RNAi (applied at either L1 or young adult stages),
599 and *lgg-1* RNAi (applied at the young adult stage) worms co-treated with bortezomib (Btz) in
600 the presence or absence of FUdR, as depicted by using anti-GFP antibody. The No-Stain
601 Protein Labeling Reagent was used to confirm equal protein loading. **(C)** Western blot showing
602 degradation of UbV-GFP upon RNAi depletion of *fem-1* in control worms, with or without
603 bortezomib (Btz) or FUdR, as depicted by using anti-GFP antibody. The No-Stain Protein
604 Labeling Reagent was used to confirm equal protein loading. **(D)** FUdR's effect on proteasome
605 activity, as measured by trypsin-like, chymotrypsin-like, and caspase-like activity in *skn-1*
606 silenced worms with or without FUdR treatment. Proteasome activity is represented as slopes
607 obtained from kinetic measurements. The experiments were conducted thrice as separate
608 biological replicates, and significance levels (ns - not significant) were determined using an
609 unpaired t-test with Welch's correction.

610 **Figure S3. Impact of FUdR in the absence of proteasome subunits on longevity and cold**
611 **survival. (A)** The lifespan of wild-type worms when exposed to *pas-1* or *pbs-2* RNAi in the
612 presence or absence FUdR. Number of worms used in the study: *pas-1* RNAi: n=171 (+ FUdR)
613 or n=171 (- FUdR); *pbs-2* RNAi: n=147 (+ FUdR) or n=194 (- FUdR). **(B)** The impact of FUdR
614 on the cold survival of wild-type and *pbs-6* knockdown worms, with or without a cold
615 adaptation period. Data was analyzed using two-way ANOVA and the significance levels
616 obtained from the Šidák's multiple comparisons test are indicated for the compared conditions
617 (ns - not significant, **** - $P \leq 0.0001$). **(C)** The impact of FUdR on the cold survival of wild-
618 type and *pbs-6* tissue-specific knockdown worms, with or without a cold adaptation period.
619 Data was analyzed using two-way ANOVA and the significance levels obtained from the
620 Šidák's multiple comparisons test are indicated for the compared conditions (ns - not

621 significant, ** - $P \leq 0.01$, *** - $P \leq 0.001$). In panels B-C, at least 90 animals were scored in three
622 independent biological replicates.

623 **Figure S4. FUdR activates a detoxification pathway involving GST-24 to regulate the**
624 **UPS. (A)** Venn diagram showing the abundance of proteins up-regulated exclusively in the
625 presence of FUdR in wild-type, *glp-1(e2144)* and *skn-1 (mg570)* worms. **(B)** Western blot
626 showing the impact of bacterial viability on the UbV-GFP reporter turnover in the presence of
627 bortezomib (Btz) and FUdR, as depicted by using anti-GFP antibody. The No-Stain Protein
628 Labeling Reagent was used to confirm equal protein loading. **(C)** *In vivo* UPS activity assay
629 showing the effect of FUdR and RNAi knockdown of detoxification-associated proteins GST-
630 24, UGT-39, UGT-48, CYP35A3, and CYP14A5 on UbV-GFP turnover. **(D)** The impact of
631 FUdR on the cold survival of wild-type and *skn-1(mg570)* worms subjected to control, *pbs-6*
632 and *gst-24* RNAi. Data was analyzed using two-way ANOVA and the significance levels
633 obtained from the Šidák's multiple comparisons test are indicated for the compared conditions
634 (ns - not significant, **** - $P \leq 0.0001$). At least 90 animals were scored in three independent
635 biological replicates. **(E)** *In vivo* UPS activity assay showing the effect of FUdR and RNAi
636 knockdown of neuronal ciliary components *che-12* and *che-13*, either individually or in
637 combination with *skn-1* RNAi, on UbV-GFP turnover. In panels C and E, the scale bar
638 corresponds to 400 μm.

639 **REFERENCES**

640 1. Hoppe T, Cohen E. Organismal Protein Homeostasis Mechanisms. Genetics.
641 2020;215(4):889-901.
642 2. Kaushik S, Cuervo AM. Proteostasis and aging. Nat Med. 2015;21(12):1406-15.
643 3. Hipp MS, Kasturi P, Hartl FU. The proteostasis network and its decline in ageing. Nat
644 Rev Mol Cell Biol. 2019;20(7):421-35.
645 4. Kurtishi A, Rosen B, Patil KS, Alves GW, Moller SG. Cellular Proteostasis in
646 Neurodegeneration. Mol Neurobiol. 2019;56(5):3676-89.
647 5. Antebi A. Regulation of longevity by the reproductive system. Exp Gerontol.
648 2013;48(7):596-602.
649 6. Kimble J, Crittenden SL. Controls of germline stem cells, entry into meiosis, and the
650 sperm/oocyte decision in Caenorhabditis elegans. Annu Rev Cell Dev Biol. 2007;23:405-33.

651 7. Austin J, Kimble J. glp-1 is required in the germ line for regulation of the decision
652 between mitosis and meiosis in C. elegans. Cell. 1987;51(4):589-99.
653 8. Grushko D, Boocholez H, Levine A, Cohen E. Temporal requirements of SKN-1/NRF
654 as a regulator of lifespan and proteostasis in Caenorhabditis elegans. PLoS One.
655 2021;16(7):e0243522.
656 9. Chondrogianni N, Georgila K, Kourtis N, Tavernarakis N, Gonos ES. 20S proteasome
657 activation promotes life span extension and resistance to proteotoxicity in Caenorhabditis
658 elegans. FASEB J. 2015;29(2):611-22.
659 10. Berman JR, Kenyon C. Germ-cell loss extends C. elegans life span through regulation
660 of DAF-16 by kri-1 and lipophilic-hormone signaling. Cell. 2006;124(5):1055-68.
661 11. O'Brien D, Jones LM, Good S, Miles J, Vijayabaskar MS, Aston R, et al. A PQM-1-
662 Mediated Response Triggers Transcellular Chaperone Signaling and Regulates Organismal
663 Proteostasis. Cell Rep. 2018;23(13):3905-19.
664 12. Lapierre LR, Gelino S, Melendez A, Hansen M. Autophagy and lipid metabolism
665 coordinately modulate life span in germline-less C. elegans. Curr Biol. 2011;21(18):1507-14.
666 13. Shemesh N, Shai N, Ben-Zvi A. Germline stem cell arrest inhibits the collapse of
667 somatic proteostasis early in Caenorhabditis elegans adulthood. Aging Cell. 2013;12(5):814-
668 22.
669 14. Steinbaugh MJ, Narasimhan SD, Robida-Stubbs S, Moronetti Mazzeo LE, Dreyfuss
670 JM, Hourihan JM, et al. Lipid-mediated regulation of SKN-1/Nrf in response to germ cell
671 absence. Elife. 2015;4.
672 15. McColl G, Rogers AN, Alavez S, Hubbard AE, Melov S, Link CD, et al. Insulin-like
673 signaling determines survival during stress via posttranscriptional mechanisms in C. elegans.
674 Cell Metab. 2010;12(3):260-72.
675 16. Gandhi S, Santelli J, Mitchell DH, Stiles JW, Sanadi DR. A simple method for
676 maintaining large, aging populations of Caenorhabditis elegans. Mech Ageing Dev.
677 1980;12(2):137-50.
678 17. Van Raamsdonk JM, Hekimi S. FUdR causes a twofold increase in the lifespan of the
679 mitochondrial mutant gas-1. Mech Ageing Dev. 2011;132(10):519-21.
680 18. Aitlhadj L, Sturzenbaum SR. The use of FUdR can cause prolonged longevity in mutant
681 nematodes. Mech Ageing Dev. 2010;131(5):364-5.
682 19. Anderson EN, Corkins ME, Li JC, Singh K, Parsons S, Tucey TM, et al. C. elegans
683 lifespan extension by osmotic stress requires FUdR, base excision repair, FOXO, and sirtuins.
684 Mech Ageing Dev. 2016;154:30-42.
685 20. Angeli S, Klang I, Sivapatham R, Mark K, Zucker D, Bhaumik D, et al. A DNA
686 synthesis inhibitor is protective against proteotoxic stressors via modulation of fertility
687 pathways in Caenorhabditis elegans. Aging (Albany NY). 2013;5(10):759-69.
688 21. Brunquell J, Bowers P, Westerheide SD. Fluorodeoxyuridine enhances the heat shock
689 response and decreases polyglutamine aggregation in an HSF-1-dependent manner in
690 Caenorhabditis elegans. Mech Ageing Dev. 2014;141-142:1-4.
691 22. Feldman N, Kosolapov L, Ben-Zvi A. Fluorodeoxyuridine improves Caenorhabditis
692 elegans proteostasis independent of reproduction onset. PLoS One. 2014;9(1):e85964.
693 23. Davies SK, Leroi AM, Bundy JG. Fluorodeoxyuridine affects the identification of
694 metabolic responses to daf-2 status in Caenorhabditis elegans. Mech Ageing Dev.
695 2012;133(1):46-9.
696 24. Yoshioka A, Tanaka S, Hiraoka O, Koyama Y, Hirota Y, Ayusawa D, et al.
697 Deoxyribonucleoside triphosphate imbalance. 5-Fluorodeoxyuridine-induced DNA double
698 strand breaks in mouse FM3A cells and the mechanism of cell death. J Biol Chem.
699 1987;262(17):8235-41.

25. Vermezovic J, Stergiou L, Hengartner MO, d'Adda di Fagagna F. Differential regulation of DNA damage response activation between somatic and germline cells in Caenorhabditis elegans. Cell Death Differ. 2012;19(11):1847-55.
26. Lee HJ, Alirzayeva H, Koyuncu S, Rueber A, Noormohammadi A, Vilchez D. Cold temperature extends longevity and prevents disease-related protein aggregation through PA28gamma-induced proteasomes. Nat Aging. 2023;3(5):546-66.
27. Habacher C, Guo Y, Venz R, Kumari P, Neagu A, Gaidatzis D, et al. Ribonuclease-Mediated Control of Body Fat. Dev Cell. 2016;39(3):359-69.
28. Vilchez D, Morantte I, Liu Z, Douglas PM, Merkwirth C, Rodrigues AP, et al. RPN-6 determines C. elegans longevity under proteotoxic stress conditions. Nature. 2012;489(7415):263-8.
29. Gu T, Orita S, Han M. Caenorhabditis elegans SUR-5, a novel but conserved protein, negatively regulates LET-60 Ras activity during vulval induction. Mol Cell Biol. 1998;18(8):4556-64.
30. Segref A, Torres S, Hoppe T. A screenable in vivo assay to study proteostasis networks in Caenorhabditis elegans. Genetics. 2011;187(4):1235-40.
31. Dantuma NP, Lindsten K, Glas R, Jellne M, Masucci MG. Short-lived green fluorescent proteins for quantifying ubiquitin/proteasome-dependent proteolysis in living cells. Nat Biotechnol. 2000;18(5):538-43.
32. Garcia-Gonzalez AP, Ritter AD, Shrestha S, Andersen EC, Yilmaz LS, Walhout AJM. Bacterial Metabolism Affects the C. elegans Response to Cancer Chemotherapeutics. Cell. 2017;169(3):431-41 e8.
33. Ghazi A, Henis-Korenblit S, Kenyon C. Regulation of Caenorhabditis elegans lifespan by a proteasomal E3 ligase complex. Proc Natl Acad Sci U S A. 2007;104(14):5947-52.
34. Robinson JD, Powell JR. Long-term recovery from acute cold shock in Caenorhabditis elegans. BMC Cell Biol. 2016;17:2.
35. Rogers AN, Chen D, McColl G, Czerwieniec G, Felkey K, Gibson BW, et al. Life span extension via eIF4G inhibition is mediated by posttranscriptional remodeling of stress response gene expression in C. elegans. Cell Metab. 2011;14(1):55-66.
36. Howard AC, Rollins J, Snow S, Castor S, Rogers AN. Reducing translation through eIF4G/IFG-1 improves survival under ER stress that depends on heat shock factor HSF-1 in Caenorhabditis elegans. Aging Cell. 2016;15(6):1027-38.
37. Advani VM, Ivanov P. Translational Control under Stress: Reshaping the Translatome. Bioessays. 2019;41(5):e1900009.
38. Roux PP, Topisirovic I. Signaling Pathways Involved in the Regulation of mRNA Translation. Mol Cell Biol. 2018;38(12).
39. Seo K, Choi E, Lee D, Jeong DE, Jang SK, Lee SJ. Heat shock factor 1 mediates the longevity conferred by inhibition of TOR and insulin/IGF-1 signaling pathways in C. elegans. Aging Cell. 2013;12(6):1073-81.
40. Lan J, Rollins JA, Zang X, Wu D, Zou L, Wang Z, et al. Translational Regulation of Non-autonomous Mitochondrial Stress Response Promotes Longevity. Cell Rep. 2019;28(4):1050-62 e6.
41. Joshi KK, Matlack TL, Rongo C. Dopamine signaling promotes the xenobiotic stress response and protein homeostasis. EMBO J. 2016;35(17):1885-901.
42. Guerrero GA, Derisbourg MJ, Mayr FA, Wester LE, Giorda M, Dinort JE, et al. NHR-8 and P-glycoproteins uncouple xenobiotic resistance from longevity in chemosensory C. elegans mutants. Elife. 2021;10.
43. Perkins LA, Hedgecock EM, Thomson JN, Culotti JG. Mutant sensory cilia in the nematode Caenorhabditis elegans. Dev Biol. 1986;117(2):456-87.

749 44. Li X, Matilainen O, Jin C, Glover-Cutter KM, Holmberg CI, Blackwell TK. Specific
750 SKN-1/Nrf stress responses to perturbations in translation elongation and proteasome activity.
751 PLoS Genet. 2011;7(6):e1002119.
752 45. An JH, Vranas K, Lucke M, Inoue H, Hisamoto N, Matsumoto K, et al. Regulation of
753 the Caenorhabditis elegans oxidative stress defense protein SKN-1 by glycogen synthase
754 kinase-3. Proc Natl Acad Sci U S A. 2005;102(45):16275-80.
755 46. Detienne G, Van de Walle P, De Haes W, Schoofs L, Temmerman L. SKN-1-
756 independent transcriptional activation of glutathione S-transferase 4 (GST-4) by EGF
757 signaling. Worm. 2016;5(4):e1230585.
758 47. Kahn NW, Rea SL, Moyle S, Kell A, Johnson TE. Proteasomal dysfunction activates
759 the transcription factor SKN-1 and produces a selective oxidative-stress response in
760 Caenorhabditis elegans. Biochem J. 2008;409(1):205-13.
761 48. Leiers B, Kampkotter A, Grevelding CG, Link CD, Johnson TE, Henkle-Duhrsen K. A
762 stress-responsive glutathione S-transferase confers resistance to oxidative stress in
763 Caenorhabditis elegans. Free Radic Biol Med. 2003;34(11):1405-15.
764 49. Ermolaeva MA, Segref A, Dakhovnik A, Ou HL, Schneider JI, Utermohlen O, et al.
765 DNA damage in germ cells induces an innate immune response that triggers systemic stress
766 resistance. Nature. 2013;501(7467):416-20.
767 50. Jiang W, Wei Y, Long Y, Owen A, Wang B, Wu X, et al. A genetic program mediates
768 cold-warming response and promotes stress-induced phenoptosis in C. elegans. Elife. 2018;7.
769 51. Murray P, Hayward SA, Govan GG, Gracey AY, Cossins AR. An explicit test of the
770 phospholipid saturation hypothesis of acquired cold tolerance in Caenorhabditis elegans. Proc
771 Natl Acad Sci U S A. 2007;104(13):5489-94.
772 52. Anderson SM, Cheesman HK, Peterson ND, Salisbury JE, Soukas AA, Pukkila-Worley
773 R. The fatty acid oleate is required for innate immune activation and pathogen defense in
774 Caenorhabditis elegans. PLoS Pathog. 2019;15(6):e1007893.
775 53. Pekec T, Lewandowski J, Komur AA, Sobanska D, Guo Y, Switonska-Kurkowska K,
776 et al. Ferritin-mediated iron detoxification promotes hypothermia survival in Caenorhabditis
777 elegans and murine neurons. Nat Commun. 2022;13(1):4883.
778 54. Martineau CN, Kirienko NV, Pujol N. Innate immunity in C. elegans. Curr Top Dev
779 Biol. 2021;144:309-51.
780 55. O'Neil BH, Raftery L, Calvo BF, Chakravarthy AB, Ivanova A, Myers MO, et al. A
781 phase I study of bortezomib in combination with standard 5-fluorouracil and external-beam
782 radiation therapy for the treatment of locally advanced or metastatic rectal cancer. Clin
783 Colorectal Cancer. 2010;9(2):119-25.
784 56. Wang HF, Tong Y, Liu L, Liu HP, Li CD, Liu QR. The effects of bortezomib alone or
785 in combination with 5-fluorouracil on proliferation and apoptosis of choriocarcinoma cells. Eur
786 J Gynaecol Oncol. 2016;37(5):627-31.
787 57. Brenner S. The genetics of Caenorhabditis elegans. Genetics. 1974;77(1):71-94.
788 58. Beydoun S, Choi HS, Dela-Cruz G, Kruempel J, Huang S, Bazopoulou D, et al. An
789 alternative food source for metabolism and longevity studies in Caenorhabditis elegans.
790 Commun Biol. 2021;4(1):258.
791 59. Zou L, Wu D, Zang X, Wang Z, Wu Z, Chen D. Construction of a germline-specific
792 RNAi tool in C. elegans. Sci Rep. 2019;9(1):2354.
793 60. Qadota H, Inoue M, Hikita T, Koppen M, Hardin JD, Amano M, et al. Establishment
794 of a tissue-specific RNAi system in C. elegans. Gene. 2007;400(1-2):166-73.
795 61. Espelt MV, Estevez AY, Yin X, Strange K. Oscillatory Ca2+ signaling in the isolated
796 Caenorhabditis elegans intestine: role of the inositol-1,4,5-trisphosphate receptor and
797 phospholipases C beta and gamma. J Gen Physiol. 2005;126(4):379-92.

798 62. Calixto A, Chelur D, Topalidou I, Chen X, Chalfie M. Enhanced neuronal RNAi in C.
799 elegans using SID-1. Nat Methods. 2010;7(7):554-9.
800 63. Kamath RS, Ahringer J. Genome-wide RNAi screening in Caenorhabditis elegans.
801 Methods. 2003;30(4):313-21.
802 64. Ravi V, Jain A, Mishra S, Sundaresan NR. Measuring Protein Synthesis in Cultured
803 Cells and Mouse Tissues Using the Non-radioactive SUnSET Assay. Curr Protoc Mol Biol.
804 2020;133(1):e127.
805 65. Doellinger J, Schneider A, Hoeller M, Lasch P. Sample Preparation by Easy Extraction
806 and Digestion (SPEED) - A Universal, Rapid, and Detergent-free Protocol for Proteomics
807 Based on Acid Extraction. Mol Cell Proteomics. 2020;19(1):209-22.
808 66. Myers SA, Rhoads A, Cocco AR, Peckner R, Haber AL, Schweitzer LD, et al.
809 Streamlined Protocol for Deep Proteomic Profiling of FAC-sorted Cells and Its Application to
810 Freshly Isolated Murine Immune Cells. Mol Cell Proteomics. 2019;18(5):995-1009.
811 67. Tyanova S, Temu T, Cox J. The MaxQuant computational platform for mass
812 spectrometry-based shotgun proteomics. Nat Protoc. 2016;11(12):2301-19.
813 68. Tyanova S, Temu T, Sinitcyn P, Carlson A, Hein MY, Geiger T, et al. The Perseus
814 computational platform for comprehensive analysis of (prote)omics data. Nat Methods.
815 2016;13(9):731-40.
816 69. Deutsch EW, Csordas A, Sun Z, Jarnuczak A, Perez-Riverol Y, Ternent T, et al. The
817 ProteomeXchange consortium in 2017: supporting the cultural change in proteomics public
818 data deposition. Nucleic Acids Res. 2017;45(D1):D1100-D6.
819 70. Perez-Riverol Y, Bai J, Bandla C, Garcia-Seisdedos D, Hewapathirana S,
820 Kamatchinathan S, et al. The PRIDE database resources in 2022: a hub for mass spectrometry-
821 based proteomics evidences. Nucleic Acids Res. 2022;50(D1):D543-D52.
822

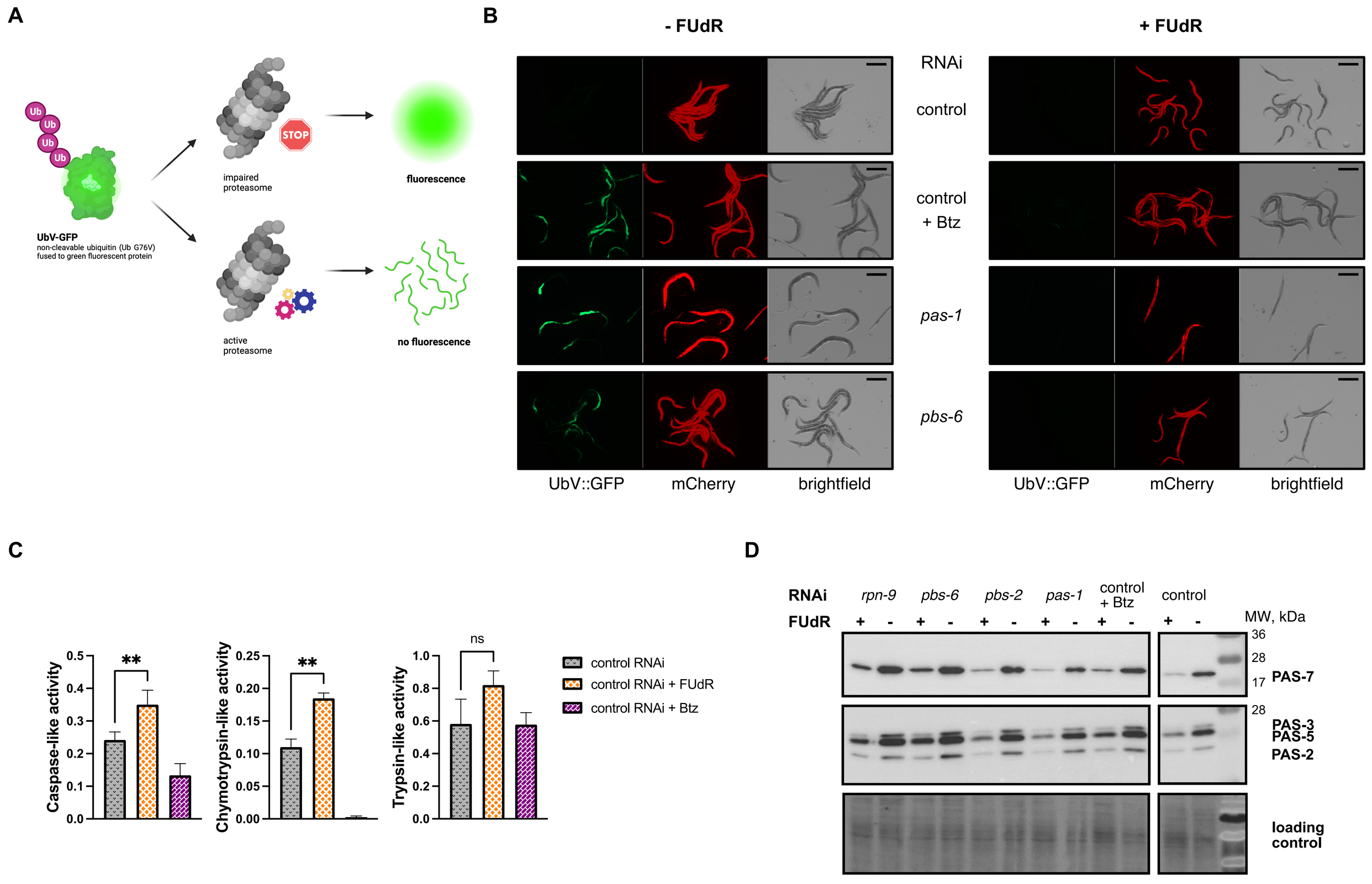

Figure 1. Enhancement of proteasome activity by FUdR. (A) A scheme illustrating the method for monitoring *in vivo* UPS activity, employing UbV-GFP as the indicative reporter. **(B)** *In vivo* UPS activity assay showing the effect of FUdR on UbV-GFP turnover in the presence of the proteasome inhibitor bortezomib (Btz) and during the RNAi depletion of *pas-1* and *pbs-6* proteasome subunits. Scale bar corresponds to 400 μm. **(C)** FUdR's effect on proteasome activity, as measured by trypsin-like, chymotrypsin-like, and caspase-like activity in wild-type worms with or without FUdR treatment. Bortezomib (Btz) served as the negative control. Proteasome activity is represented as slopes obtained from kinetic measurements. The experiments were conducted thrice as separate biological replicates, and significance levels (** - $P \leq 0.01$) were determined using an unpaired t-test with Welch's correction. **(D)** Western blot showing levels of PAS-2, PAS-3, PAS-5, and PAS-7 proteasome subunits levels in wild-type worms following the RNAi depletion of RPN-9, PBS-6, PBS-2 and PAS-1 proteasome components in the presence or absence of FUdR, as depicted by using anti-proteasome 20S alpha 1+2+3+5+6+7 antibody. The No-Stain Protein Labeling Reagent was used to confirm equal protein loading.

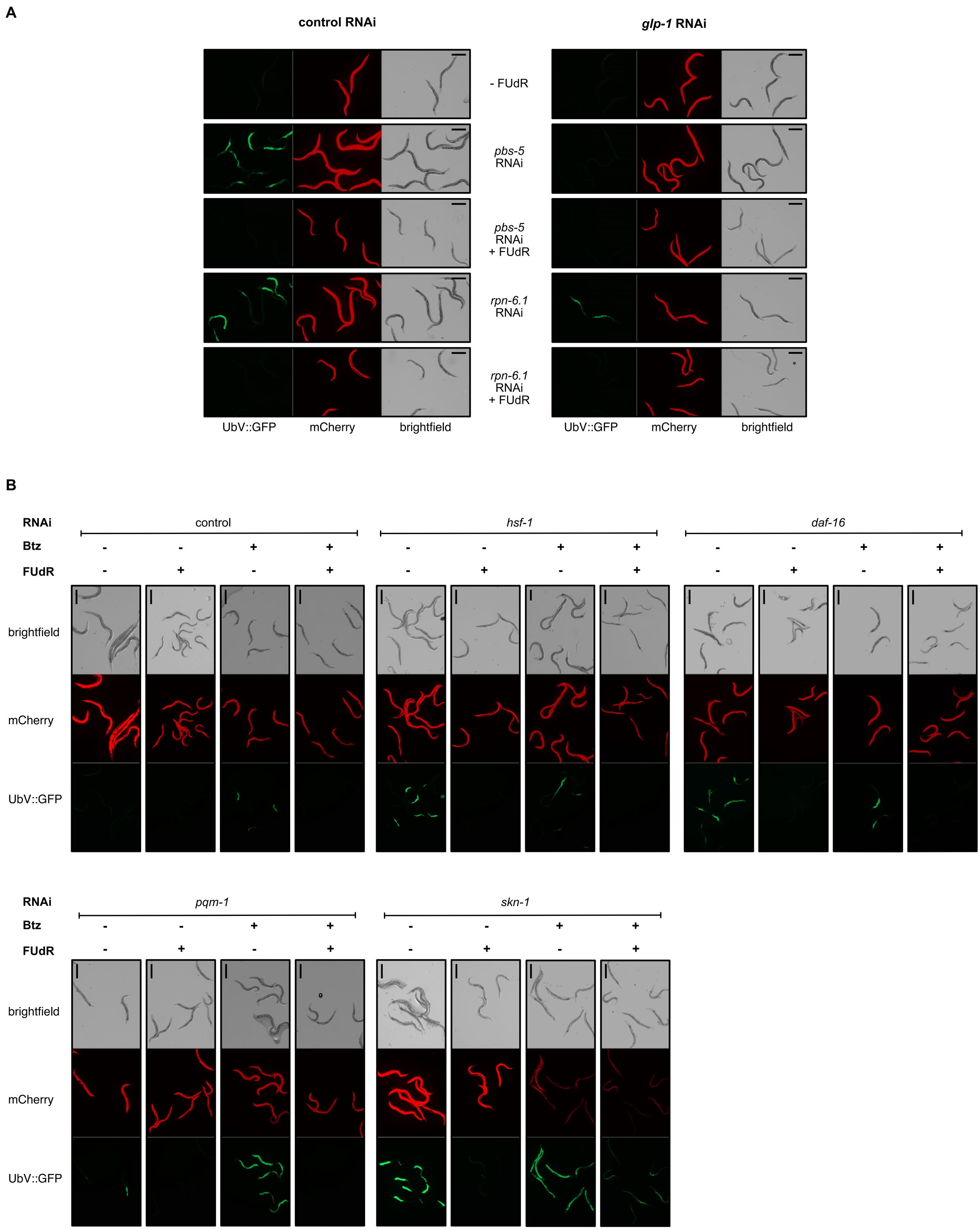

Figure 2. The improved UPS activity mediated by FUdR partially relies on *skn-1*. (A) *In vivo* UPS activity assay showing the effect of FUdR on UbV-GFP turnover in worms subjected to *glp-1*, *pbs-5* and *rpn-6.1* RNAi silencing, with or without FUdR. **(B)** *In vivo* UPS activity assay showing the effect of FUdR on UbV-GFP turnover in worms subjected to *hsf-1*, *daf-16*, *pqm-1*, and *skn-1* RNAi silencing in the absence or presence of bortezomib (Btz). In panels A and B, the scale bar corresponds to 400 µm.

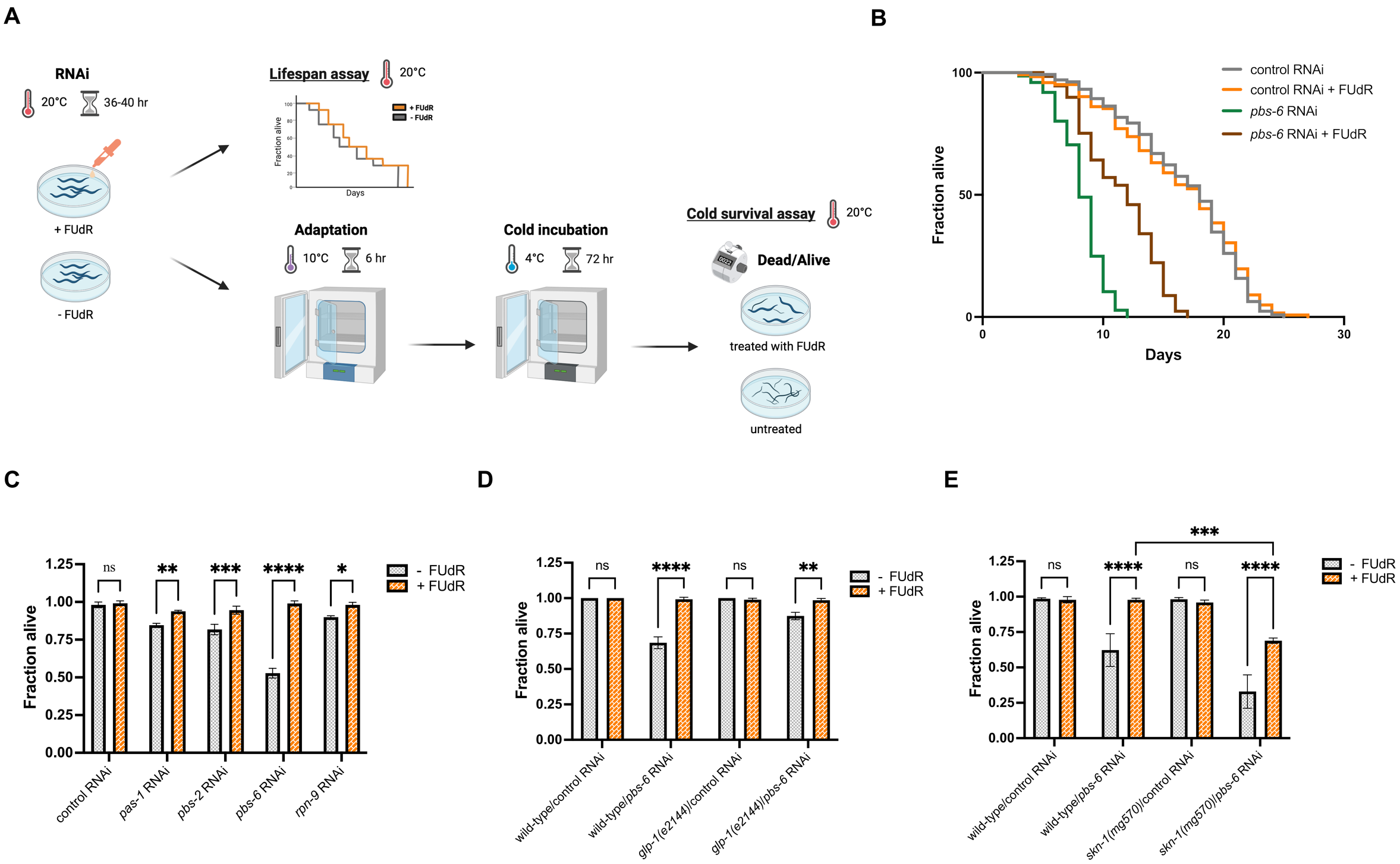

Figure 3. FUdR enhances lifespan and cold survival upon proteasome deficits. (A) A schematic representation of cold survival and lifespan assays. **(B)** The lifespan of wild-type worms when exposed to control or *pbs-6* RNAi in the presence or absence FUdR. Number of worms used in the study: control RNAi: n=123 (+ FUdR) or n=139 (- FUdR); *pbs-6* RNAi: n=129 (+ FUdR) or n=149 (- FUdR). **(C)** The impact of FUdR on the cold survival rate of wild-type worms during the knockdown of PAS-1, PBS-2, PBS-6, and RPN-9, considering both FUdR-treated and untreated conditions. Data was analyzed using two-way ANOVA and the significance levels obtained from the Šidák's multiple comparisons test are indicated for the compared conditions (ns - not significant, * - $P \leq 0.05$, ** - $P \leq 0.01$, *** - $P \leq 0.001$, **** - $P \leq 0.0001$). **(D)** The impact of FUdR on the cold survival of wild-type and *glp-1(e2144)* worms subjected to control and *pbs-6* RNAi. Data was analyzed using two-way ANOVA and the significance levels obtained from the Šidák's multiple comparisons test are indicated for the compared conditions (ns - not significant, ** - $P \leq 0.01$, **** - $P \leq 0.0001$). **(E)** The impact of FUdR on the cold survival of wild-type and *skn-1(mg570)* worms subjected to control and *pbs-6* RNAi. Data was analyzed using two-way ANOVA and the significance levels obtained from the Tukey's multiple comparisons test are indicated for the compared conditions (ns - not significant, *** - $P \leq 0.001$, **** - $P \leq 0.0001$). In panels C-E, at least 90 animals were scored in three independent biological replicates.

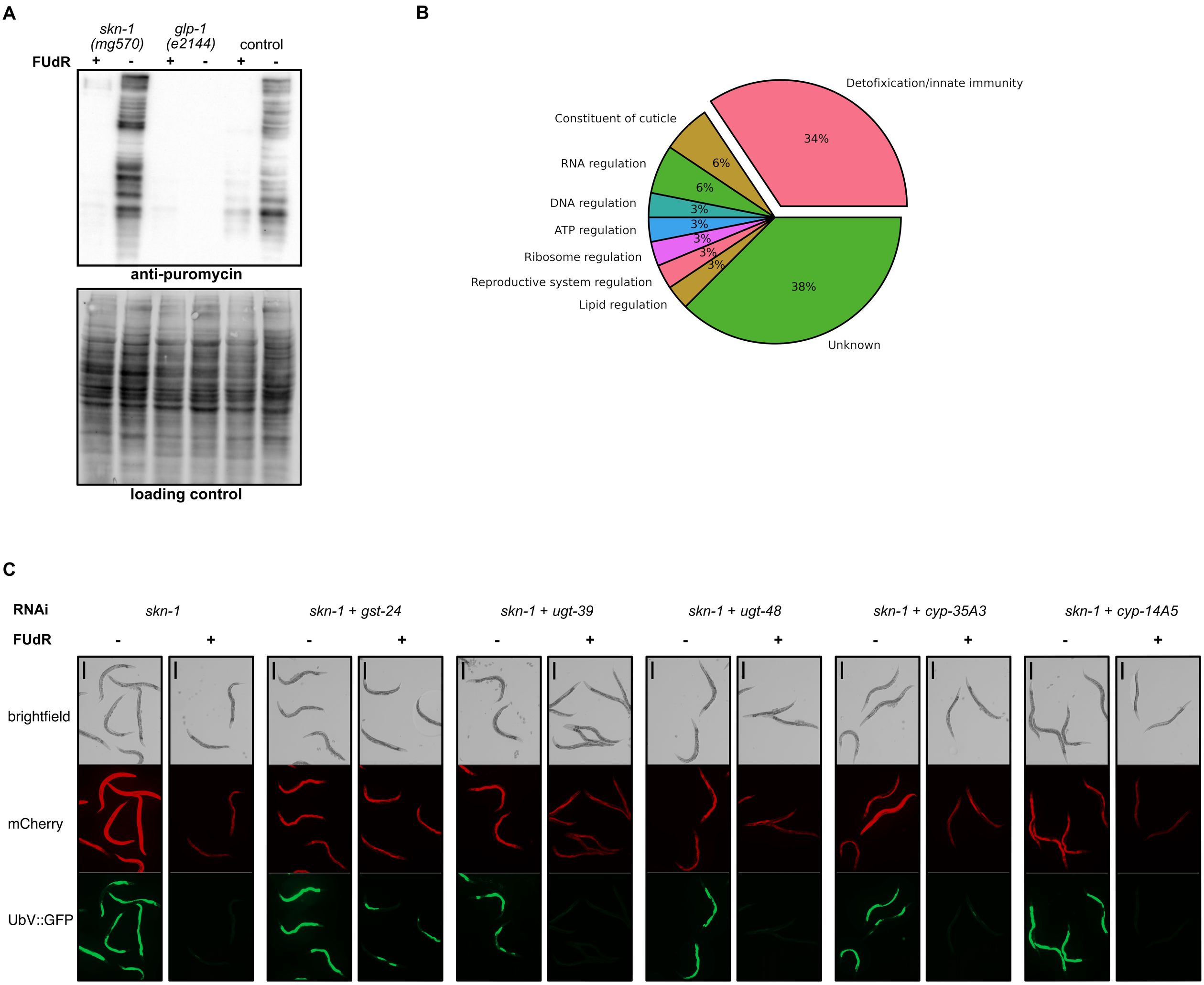

Figure 4. FUdR promotes detoxification pathway independent of *skn-1* and *glp-1*. (A) Western blot showing global translation activity in wild-type, *glp-1(e2144)*, and *skn-1(mg570)* worms, in the presence or absence of FUdR, as depicted by using anti-puromycin antibody. The No-Stain Protein Labeling Reagent was used to confirm equal protein loading. **(B)** Pie chart representing the functional categories of proteins from our proteomics study that exhibited a marked increase (fold change > 1.0), observed consistently in wild-type, *glp-1(e2144)*, and *skn-1(mg570)* worms specifically due to FUdR treatment. The significance of proteomic findings was confirmed through student's t-tests, setting a *P*-value threshold < 0.05 while maintaining the false discovery rate under 0.01. Functional annotations were compiled by manual review. **(C)** *In vivo* UPS activity assay showing the effect of FUdR on UbV-GFP turnover in worms subjected to *skn-1* RNAi silencing alone or in combination with *gst-24*, *ugt-39*, *ugt-48*, *cyp35A3*, and *cyp14A5* RNAi silencing, with or without FUdR. Scale bar corresponds to 400 μm.

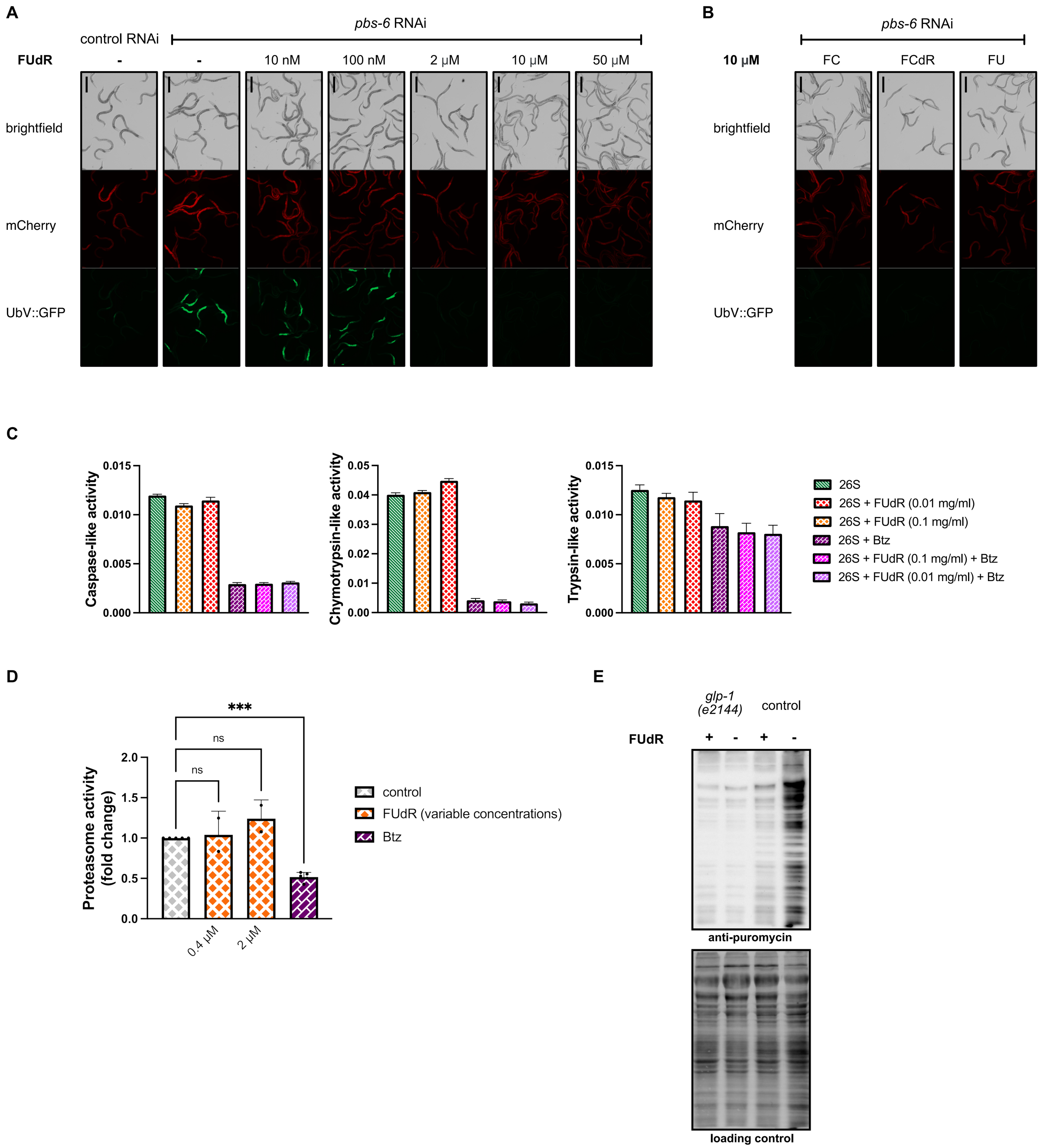

Figure S1. **Pyrimidine analogs improve UPS activity. (A)** *In vivo* UPS activity assay showing the effect of different concentrations of FUdR on UbV-GFP turnover. **(B)** *In vivo* UPS activity assay showing the effect of different pyrimidine analogs, 5-fluorouracil (FU), 5-fluorocytosine (FC), and 5-fluorodeoxycytidine (FCdR), on UbV-GFP turnover. In panels A and B, the scale bar corresponds to 400 μm. **(C)** Effect of different concentrations of FUdR on the activity of purified human 26S proteasome in HeLa cells, as measured by trypsin-like, chymotrypsin-like, and caspase-like activity in wild-type worms with or without FUdR treatment. Bortezomib (Btz) served as the negative control. Proteasome activity is represented as slopes obtained from kinetic measurements. The experiments were conducted thrice as separate biological replicates. **(D)** FUdR effect on chymotrypsin-like proteasome activity in HeLa cells. Cells were treated with final concentrations of 0.4 and 2 μM of FUdR and 10 nM bortezomib (Btz) as control for 6 hr. The assay was conducted by incubating the cells with 100 μl Proteasome Assay Loading Solution for 2 h as described in the methods. Results from three technical replicates were corrected for background by subtracting the fluorescence of the medium without cells and further normalized to dimethyl sulfoxide control. The graph shows the average values obtained from either two or four biological replicates for experiments that involve FUdR or Btz, respectively. **(E)** Western blot showing global translation activity in wild-type and *glp-1(e2144)* worms, in the presence or absence of FUdR, as depicted by using the anti-puromycin antibody. The No-Stain Protein Labeling Reagent was used to confirm equal protein loading.

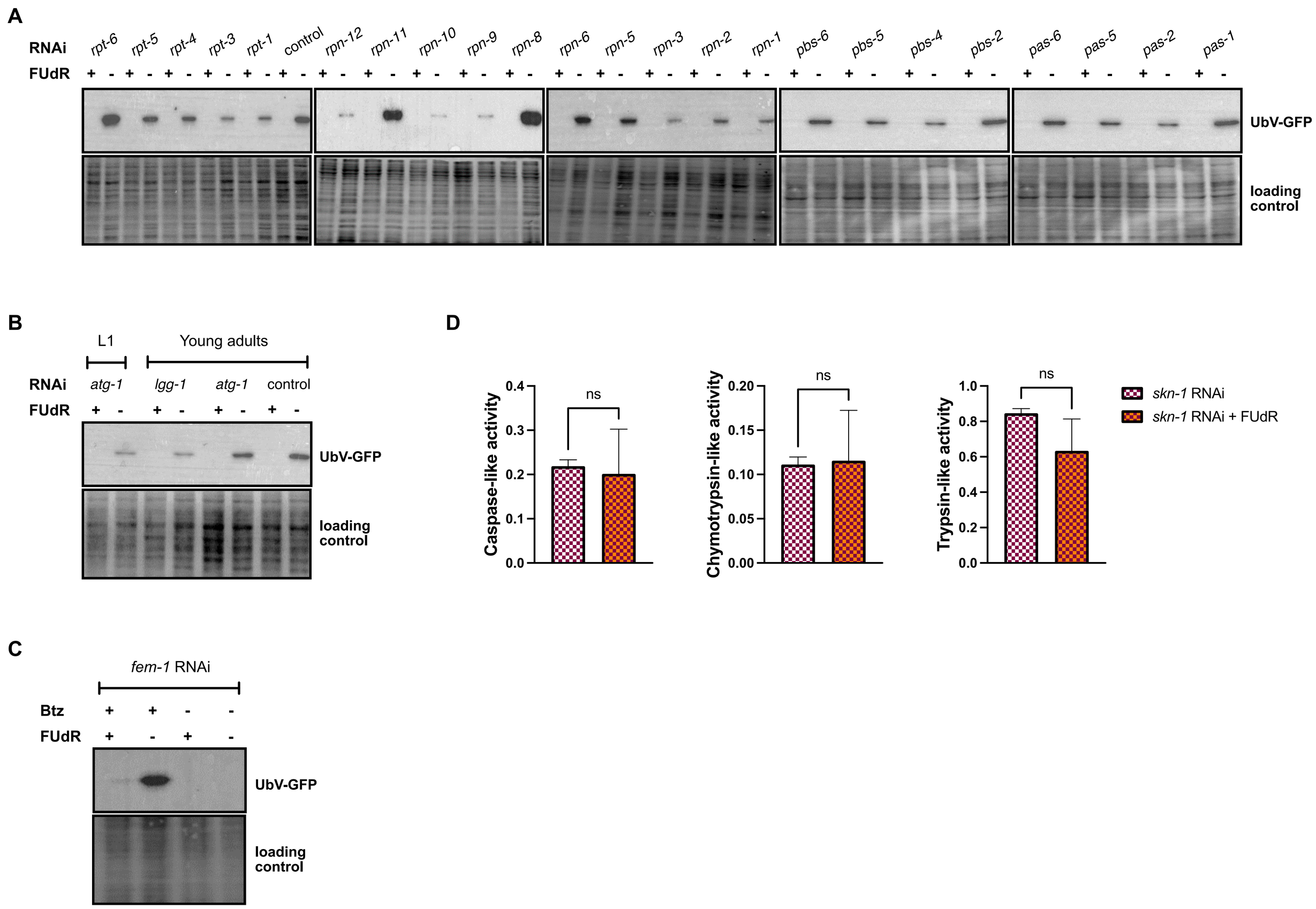

Figure S2. FUdR buffers UPS activity under proteasome-compromised conditions. (A) Western blot showing the impact of FUdR on UbV-GFP reporter turnover upon depletion of various 26S subunits in control worms, as depicted by using anti-GFP antibody. The No-Stain Protein Labeling Reagent was used to confirm equal protein loading. **(B)** Western blot showing degradation of UbV-GFP in control, *atg-1* RNAi (applied at either L1 or young adult stages), and *lgg-1* RNAi (applied at the young adult stage) worms co-treated with bortezomib (Btz) in the presence or absence of FUdR, as depicted by using anti-GFP antibody. The No-Stain Protein Labeling Reagent was used to confirm equal protein loading. **(C)** Western blot showing degradation of UbV-GFP upon RNAi depletion of *fem-1* in control worms, with or without bortezomib (Btz) or FUdR, as depicted by using anti-GFP antibody. The No-Stain Protein Labeling Reagent was used to confirm equal protein loading. (**D)** FUdR's effect on proteasome activity, as measured by trypsin-like, chymotrypsin-like, and caspase-like activity in *skn-1* silenced worms with or without FUdR treatment. Proteasome activity is represented as slopes obtained from kinetic measurements. The experiments were conducted thrice as separate biological replicates, and significance levels (ns - not significant) were determined using an unpaired t-test with Welch's correction.

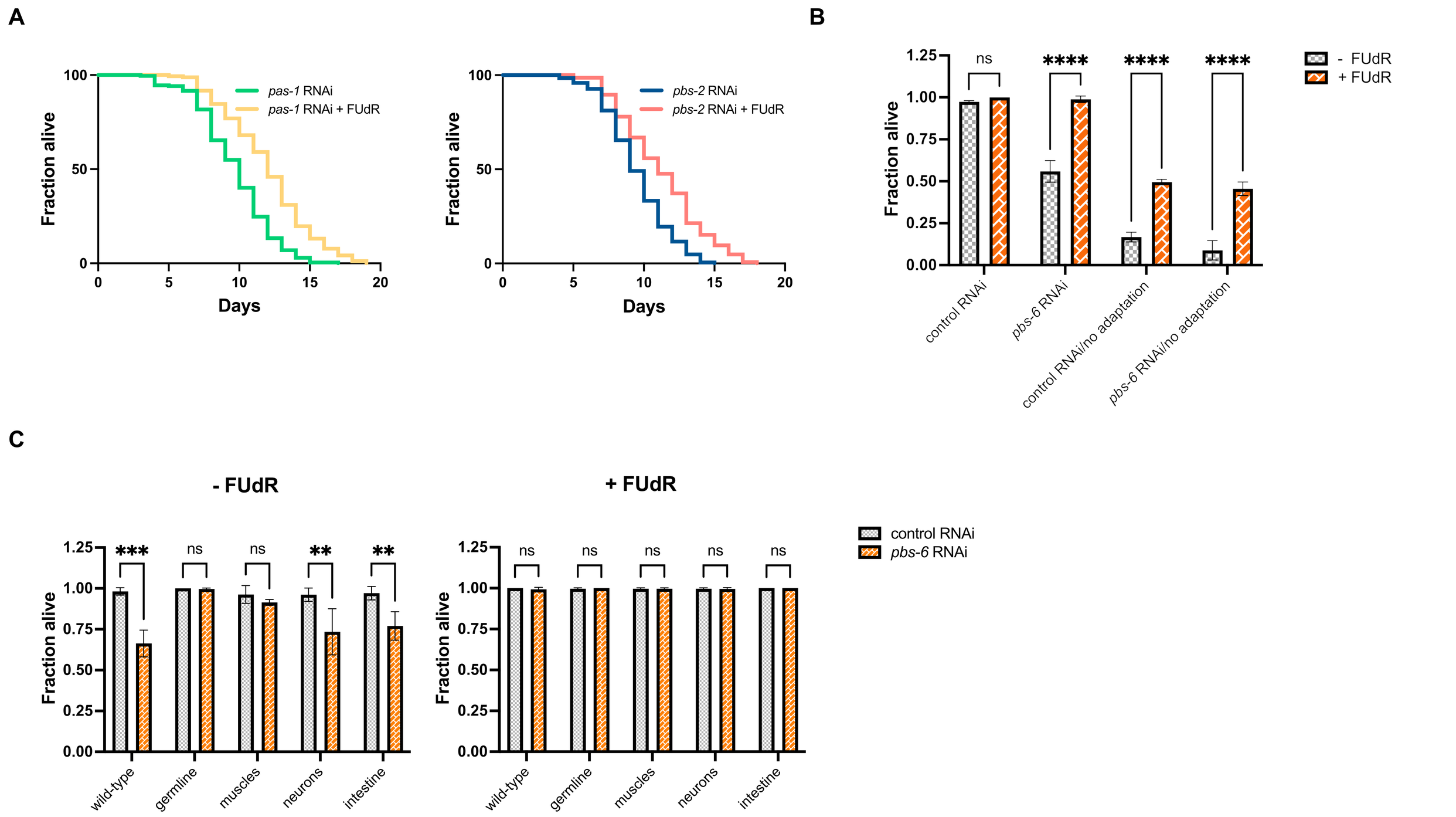

Figure S3. Impact of FUdR in the absence of proteasome subunits on longevity and cold survival. (A) The lifespan of wild-type worms when exposed to *pas-1* or *pbs-2* RNAi in the presence or absence FUdR. Number of worms used in the study: *pas-1* RNAi: n=171 (+ FUdR) or n=171 (- FUdR); *pbs-2* RNAi: n=147 (+ FUdR) or n=194 (- FUdR). **(B)** The impact of FUdR on the cold survival of wild-type and *pbs-6* knockdown worms, with or without a cold adaptation period. Data was analyzed using two-way ANOVA and the significance levels obtained from the Šidák's multiple comparisons test are indicated for the compared conditions (ns - not significant, **** - $P \leq 0.0001$). **(C)** The impact of FUdR on the cold survival of wild-type and *pbs-6* tissue-specific knockdown worms, with or without a cold adaptation period. Data was analyzed using two-way ANOVA and the significance levels obtained from the Šidák's multiple comparisons test are indicated for the compared conditions (ns - not significant, ** - $P \leq 0.01$, *** - $P \leq 0.001$). In panels B-C, at least 90 animals were scored in three independent biological replicates.

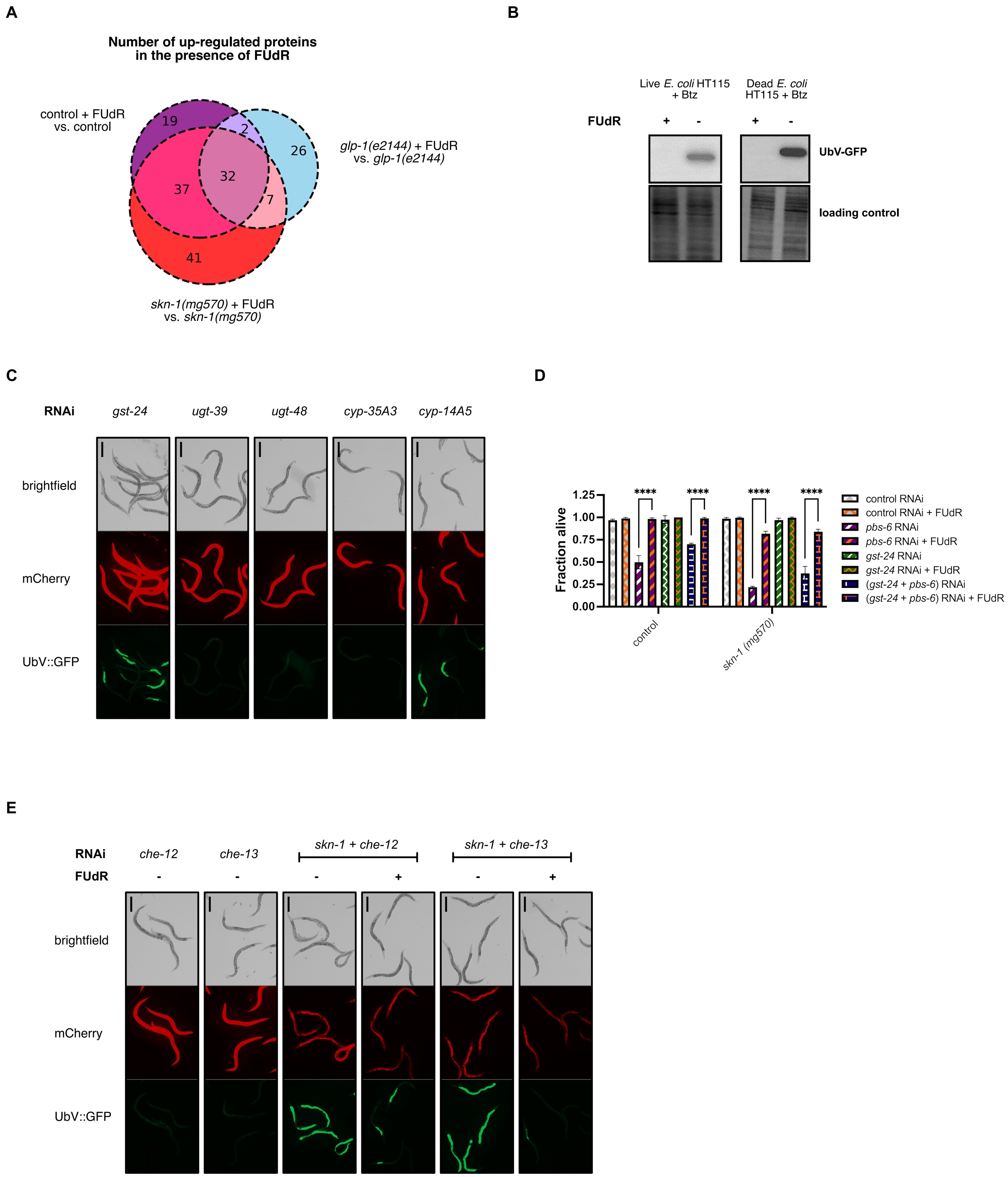

Figure S4. FUdR activates a detoxification pathway involving GST-24 to regulate the UPS. (A) Venn diagram showing the abundance of proteins up-regulated exclusively in the presence of FUdR in wild-type, *glp-1(e2144)* and *skn-1 (mg570)* worms. **(B)** Western blot showing the impact of bacterial viability on the UbV-GFP reporter turnover in the presence of bortezomib (Btz) and FUdR, as depicted by using anti-GFP antibody. The No-Stain Protein Labeling Reagent was used to confirm equal protein loading. **(C)** *In vivo* UPS activity assay showing the effect of FUdR and RNAi knockdown of detoxification-associated proteins GST-24, UGT-39, UGT-48, CYP35A3, and CYP14A5 on UbV-GFP turnover. **(D)** The impact of FUdR on the cold survival of wild-type and *skn-1(mg570)* worms subjected to control, *pbs-6* and *gst-24* RNAi. Data was analyzed using two-way ANOVA and the significance levels obtained from the Šidák's multiple comparisons test are indicated for the compared conditions (ns - not significant, **** - $P \leq 0.0001$). At least 90 animals were scored in three independent biological replicates. **(E)** *In vivo* UPS activity assay showing the effect of FUdR and RNAi knockdown of neuronal ciliary components *che-12* and *che-13*, either individually or in combination with *skn-1* RNAi, on UbV-GFP turnover. In panels C and E, the scale bar corresponds to 400 μm.